On the lateral expansion of gamma-ray burst jets

Jonathan Granot[1,2,3*] and Tsvi Piran[1]

[1]*Racah Institute of Physics, The Hebrew University, Jerusalem 91904, Israel*
[2]*Raymond and Beverly Sackler School of Physics & Astronomy, Tel Aviv University, Tel Aviv 69978, Israel*
[3]*Centre for Astrophysics Research, University of Hertfordshire, College Lane, Hatfield AL10 9AB*

ABSTRACT

The dynamics of gamma-ray burst jets during the afterglow phase have an important effect on the interpretation of their observations and for inferring key physical parameters such as their true energy and event rate. Semi-analytic models generally predict a fast lateral expansion, where the jet opening angle asymptotically grows exponentially with its radius. Numerical simulations, however, show a much more modest lateral expansion, where the jet retains memory of its initial opening angle for a very long time, and the flow remains non-spherical until it becomes subrelativistic, and only then gradually approaches spherical symmetry. Here we suggest a new analytic model based on a new physically derived recipe for the lateral expansion. We also generalize the model by relaxing the common approximations of ultrarelativistic motion and a narrow jet opening angle. We find that the new analytic model fits much better the results of numerical simulations, mainly because it remains valid also in the mildly relativistic, quasi-spherical regime. This model shows that for modest initial jet half-opening angles, θ_0, the outflow is not *sufficiently* ultrarelativistic when its Lorentz factor reaches $\Gamma = 1/\theta_0$ and therefore the sideways expansion is rather slow, showing no rapid, exponential phase. On the other hand, we find that jets with an extremely narrow initial half-opening angle, of about $\theta_0 \ll 10^{-1.5}$ or so, which are still sufficiently ultrarelativistic at $\Gamma = 1/\theta_0$, do show a phase of rapid, exponential lateral expansion. However, even such jets that expand sideways exponentially are still not spherical when they become subrelativistic.

Key words: hydrodynamics – relativistic processes – shock waves – methods: analytical – gamma-ray burst: general – ISM: jets and outflows.

1 INTRODUCTION

The ultrarelativistic outflows that power gamma-ray bursts (GRBs) are thought to be collimated into narrow jets (for reviews see Piran 2005; Granot 2007; Granot & Ramirez-Ruiz 2011). The evidence for this is rather indirect, however, since their images are usually unresolved, and in the best case (GRB 030329) the late time radio afterglow image was only marginally resolved (Frail et al. 1997; Taylor et al. 1997, 2004; Pihlström et al. 2007). The different lines of evidence for jets in GRBs include analogy to other astrophysical relativistic outflow sources such as active galactic nuclei or microquasars (e.g. Rhoads 1997), the difficulty in transferring enough energy to ultrarelativistic ejecta in a spherical explosion of a massive star (for long-duration GRBs; Tan, Matzner & McKee 2001; Perna & Vietri 2002; Granot 2007), extremely large isotropic equivalent energies in some GRBs (with $E_{\gamma,\text{iso}} \approx 4.9\,\text{M}_\odot c^2$ in GRB 080916C; Abdo et al. 2009) and an achromatic steepening of the afterglow light curves of some GRBs that is attributed to a jet (known as a

'jet break'; Rhoads 1997; Fruchter et al. 1999; Harrison et al. 1999; Kulkarni et al. 1999; Rhoads 1999; Sari, Piran & Halpern 1999; Halpern et al. 2000; Price et al. 2001). Therefore, there is very little direct observational information about the jet angular structure and dynamics, which makes it difficult to interpret GRB afterglow observations and infer from them important physical parameters such as the jet energy and opening angle, the external density profile and the microphysical parameters of the relativistic collisionless shock powering the afterglow emission.

Most studies of GRB jet dynamics during the afterglow phase have focused on a roughly uniform jet with well-defined, sharp edges. We shall also focus on such a uniform jet, and only briefly remark on the expected relation to jets with a smoother angular structure (also known as 'structured jets'). The jet dynamics have been studied both analytically (Panaitescu & Mészáros 1999; Rhoads 1999; Sari, Piran & Halpern 1999; Kumar & Panaitescu 2000; Moderski, Sikora & Bulik 2000; Piran 2000; Oren, Nakar & Piran 2004; Granot 2007) and numerically, using 2D special relativistic numerical simulations (Granot et al. 2001; Cannizzo, Gehrels & Vishniac 2004; Zhang & MacFadyen 2009; Meliani & Keppens 2010; van Eerten, Zhang & MacFadyen 2010; van Eerten

*E-mail: j.granot@herts.ac.uk

& MacFadyen 2011; Wygoda, Waxman & Frail 2011), as well as an intermediate approach where the dynamical equations are integrated over the radial profile of the thin shocked region, thus reducing the set of partial differential equations to one dimension (Kumar & Granot 2003).

Let us consider a uniform double-sided jet of total energy $E_{\rm jet}$, initial half-opening angle θ_0 and initial Lorentz factor Γ_0. GRB observations suggest that typically $\Gamma_0\theta_0 \gg 1$. At early times, as long as $\Gamma \gg \theta_0^{-1}$, the bulk of the jet is causally disconnected from its edge and thus evolves as if it where part of a spherical flow with an energy $E_{\rm iso} = (1 - \cos\theta_0)^{-1}E_{\rm jet} \approx 2\theta_0^{-2}E_{\rm jet}$, following the spherical Blandford & McKee (1976) self-similar solution. This early phase corresponds to radii $R < R_{\rm j}$, where the jet radius $R_{\rm j}$ is defined as the radius where $\Gamma = 1/\theta_0$ for a spherical flow with $E = E_{\rm iso}$. At $R > R_{\rm j}$, the bulk of the jet is in causal contact with its edge and the jet can in principal rapidly expand sideways. However, the degree of lateral spreading at this stage, which strongly affects the dynamics, is not well known. Therefore, the jet dynamics at $R > R_{\rm j}$ are still controversial. In particular, the radius $R_{\rm NR}$ at which the flow (or jet) becomes non-relativistic still remains uncertain.

The Sedov length for a spherical flow with the true jet energy, $E = E_{\rm jet}$ (i.e. the radius where it sweeps up a rest mass energy equal to its own energy and becomes non-relativistic), $R_{\rm S}(E_{\rm jet})$, is very close to $R_{\rm j}$. Therefore, in order for the jet to be already close to spherical when it becomes non-relativistic (i.e. at $R_{\rm NR}$), it must expand sideways very quickly and become close to spherical already near $R_{\rm j}$ [i.e. $R_{\rm NR}$ cannot be $\gg R_{\rm j} \sim R_{\rm S}(E_{\rm jet})$]. This is indeed roughly what happens in simple analytic models, where the jet half-opening angle, $\theta_{\rm j}$, starts growing exponentially with radius near $R_{\rm j}$, and the jet quickly becomes close to spherical and non-relativistic at a radius $R_{\rm NR} \sim (1 - \ln\theta_0)R_{\rm j} \sim (1 - \ln\theta_0)R_{\rm S}(E_{\rm jet})$, which is larger than $R_{\rm j}$ only by a logarithmic factor,[1] while at $R > R_{\rm NR}$ the flow quickly approaches the Newtonian, spherical, self-similar Sedov–Taylor solution.

Numerical simulations, however, suggest that most of the energy remains within the initial jet half-opening angle θ_0 until the flow becomes mildly relativistic, and only then does the flow start to gradually approach spherical symmetry (Granot et al. 2001; Cannizzo et al. 2004; Zhang & MacFadyen 2009; Meliani & Keppens 2010; van Eerten et al. 2010). Under the crude approximation that the jet does not expand sideways and keeps evolving as a conical section of a spherical flow up until the radius where it becomes non-relativistic, the latter is given by $R_{\rm NR} \sim R_{\rm S}(E_{\rm iso}) = \theta_0^{-2/(3-k)}R_{\rm j}$. In this case the flow is still highly non-spherical at $R_{\rm NR}$, and only very gradually approaches spherical symmetry (Granot, Ramirez-Ruiz & Loeb 2005).

This clearly shows that without lateral expansion $R_{\rm NR}$ is significantly larger, by a factor of $\sim \theta_0^{-2/(3-k)}/(1 - \ln\theta_0)$ (which is $\gg 1$ for $\theta_0 \ll 1$), than if there is fast lateral expansion at $R > R_{\rm j}$. Thus, the dynamics of the flow at small radii ($R \ll R_{\rm j}$) and at large radii [$R \gg R_{\rm S}(E_{\rm iso})$] are reasonably well known, while at intermediate radii [$R_{\rm j} \lesssim R \lesssim R_{\rm S}(E_{\rm iso})$] they are still controversial. For typical values of $\theta_0 \sim 0.1$, this range of radii may appear rather small, $R_{\rm NR}/R_{\rm j} \sim 1 - \ln\theta_0 \sim 3.3$ for exponential lateral expansion and $R_{\rm NR}/R_{\rm j} \sim \theta_0^{-2/(3-k)} \sim 4.6$ for no lateral expansion up

to $R_{\rm NR} \sim R_{\rm S}(E_{\rm iso})$ with $k = 0$. However, it corresponds to a large range in observed times (over which the corresponding afterglow emission reaches us), of $t_{\rm obs,NR}/t_{\rm obs,j} \sim (1 - \ln\theta_0)\theta_0^{-2} \sim 330$ and $\sim \theta_0^{-(8-2k)/(3-k)} \sim 460$, respectively, since the observed time scales as $t_{\rm obs} \sim R/c\Gamma^2$, and Γ decreases by a large factor (of θ_0^{-1}) within this range of radii.

Most simulations so far were for $\theta_0 = 0.2$, or even wider initial jet half-opening angles. Recently, however, Wygoda et al. (2011) and later van Eerten & MacFadyen (2011) have performed simulations also for narrower initial jets, $\theta_0 = 0.05, 0.1$ and 0.2. Wygoda et al. (2011) have found that significant lateral spreading starts when Γ drops below θ_0^{-1}, as predicted by analytic models, and tried to reconcile the apparent discrepancy with analytic models by attributing it to their small range of validity after significant lateral spreading starts ($1 \ll \Gamma < \theta_0^{-1}$) for the typical modest values of θ_0 used in the simulations. van Eerten & MacFadyen (2011) disagree with this conclusion, and we address this dispute in Section 7. More recently, Lyutikov (2011) has argued that significant lateral spreading is expected only at a later stage, when Γ drops below $\theta_0^{-1/2}$ (rather than θ_0^{-1} as obtained in simple analytic models), based on an analytic consideration (which we address in Section 3 and Appendix A, and find to be in error). Thus, there appears to be an ongoing debate on these important issues.

Here we try to reconcile the apparent differences between the analytic and numerical results, in the light of this recent debate. The different relevant critical radii are discussed in Section 2. In Section 3 we discuss the recipe for lateral expansion used by analytic models, and derive a new recipe that takes into account the non-spherical nature of the shock driven by the jet into the external medium. In Section 4 we construct an analytic relativistic model, which includes both the traditional recipe and our new recipe for the jet lateral expansion. It is also shown that while the region of interest and validity of the analytic model (corresponding to $1 \ll \Gamma < \theta_0^{-1}$) increases as θ_0 decreases, $\theta_{\rm j}$ reaches lower values, resulting in a narrower jet at the time when the analytic solution becomes invalid. Because this relativistic model breaks down in a region of interest (both for typical GRB parameters and for comparison with simulations), in Section 5 we generalize it so that it would be valid also at low Γ and high $\theta_{\rm j}$, using two different assumptions on the accumulation of the swept-up external mass (in Sections 5.1 and 5.2). According to the results of these models (Section 5.3), a phase of rapid exponential lateral expansion exists only for sufficiently narrow initial jet half-opening angles, of approximately $\theta_0 \ll 0.05, 0.03$ and 0.01 for $k = 0, 1$ and 2, respectively. In Section 6 we compare our analytic models to numerical simulations (with a modest $\theta_0 = 0.2$) and find reasonably good agreement (with no exponential lateral expansion in both cases), where the differences between the two recipes for the lateral spreading have a smaller effect on the agreement with numerical simulations compared to the generalization of the model to small Γ and large $\theta_{\rm j}$. The implications of our results are discussed in Section 7.

2 THE DIFFERENT CRITICAL RADII AND TWO EXTREME ASSUMPTIONS FOR THE JET DYNAMICS

Using the approximate equation for energy conservation (for $\Gamma \gg 1$), $E \approx \Gamma^2 M(R)c^2$, where $M(R)$ is the swept-up rest mass at radius R for a spherical flow in an external density $\rho_{\rm ext} = AR^{-k}$ (with $k < 3$), and the definition of the jet radius $R_{\rm j}$ as the radius where $\Gamma = \theta_0^{-1}$

---

[1] The mild discrepancy, by a logarithmic factor, between $R_{\rm NR}$ and $R_{\rm S}(E_{\rm jet})$ $\sim R_{\rm j}$ likely arises from the fact that in simple analytic models the swept-up mass at the radius where the jet becomes spherical is smaller than the external rest mass within a sphere of the same radius.
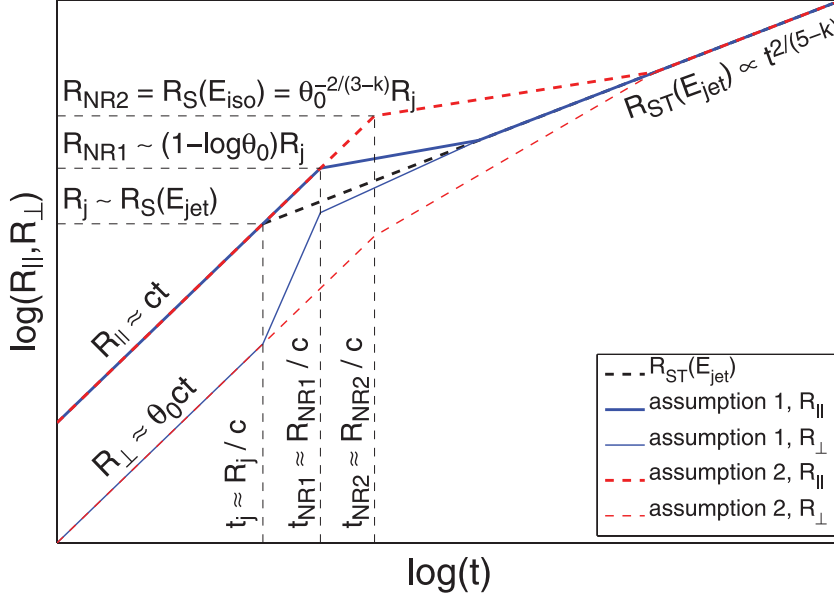
Figure 1. A schematic figure showing the evolution of the jet radius $R = R_\parallel$ (i.e. its extent along its symmetry axis) and lateral size $R_\perp$ as a function of the lab frame time t for two extreme assumptions on its degree of lateral spreading: (1) mildly relativistic lateral expansion in the jet comoving frame and (2) no lateral spreading until the jet becomes non-relativistic. The jet becomes spherical when $R_\parallel$ and $R_\perp$ become equal, which occurs well after the jet becomes non-relativistic, and then joins the Sedov–Taylor solution.

for a spherical flow of energy E_{iso}, we obtain

$$R_j = \left[\frac{(3-k)E_{jet}}{2\pi A c^2} \right]^{1/(3-k)} = 2^{1/(3-k)} R_S(E_{jet}). \quad (1)$$

Similarly, the Sedov radius of a spherical flow with $E = E_{iso}$ is

$$R_S(E_{iso}) = \left[\frac{(3-k)E_{iso}}{4\pi A c^2} \right]^{1/(3-k)} = \theta_0^{-2/(3-k)} R_j$$

$$= \left(\frac{\theta_0^2}{2} \right)^{-1/(3-k)} R_S(E_{jet}). \quad (2)$$

Two extreme assumptions on the degree of lateral spreading, which likely bracket the true jet dynamics, are (1) mildly relativistic lateral expansion in the jet comoving frame and (2) no lateral spreading until the jet becomes non-relativistic. Assumption 1, which is made in most semi-analytic models, results in exponential growth of $\theta_j(R)$, until the jet becomes quasi-spherical and non-relativistic at

$$R_{NR,1} \sim (1 - \ln\theta_0)R_j \qquad \text{(fast lateral spreading)}. \quad (3)$$

Assumption 2 was so far studied mainly by Granot et al. (2005), and leads to

$$R_{NR,2} = R_S(E_{iso}) = \theta_0^{-2/(3-k)}R_j \qquad \text{(no lateral spreading)}. \quad (4)$$

In this case the jet is still very far from spherical symmetry at R_{NR}, and thus approaches spherical symmetry only after the radius grows by a factor of b_2, of a few or several. Moreover, since the radius of the Sedov–Taylor solution scales as

$$R_{ST}(E, t) \sim R_S(E) \left[\frac{ct}{R_S(E)} \right]^{2/(5-k)} \sim \left(\frac{Et^2}{A} \right)^{1/(5-k)}, \quad (5)$$

and at the non-relativistic transition time, $t_{NR,2} \sim R_{NR,2}/c = R_S(E_{iso})/c$, the Sedov–Taylor radius of a spherical flow with the true jet energy is much smaller than the jet radius at that time,

$R_{ST}(E_{jet}, t_{NR,2})/R_{NR,2} \sim \theta_0^{-2/(5-k)} \ll 1$, the flow approaches spherical symmetry only at the time $t_{sph,2}$ when $R_{ST}(E_{jet}, t_{sph,2}) = b_2 R_{NR,2}$ $= b_2 R_S(E_{iso})$, which corresponds to $t_{sph,2}/t_{NR,2} \sim \theta_0^{-1} b_2^{(5-k)/2} \gg 1$ (see equation 6 of Granot et al. 2005). Note that $t_{sph,2}/t_{NR,2}$ is much larger than the factor (b_2) by which the radius grows over the same time. For assumption 1, similar arguments imply $t_{sph,1}/t_{NR,1} \sim (1 - \ln\theta_0)^{(3-k)/2} b_1^{(5-k)/2}$, where $b_1 < b_2$ can be expected.

Fig. 1 shows the jet radius $R = R_\parallel$ (i.e. its extent along its symmetry axis) and lateral size $R_\perp$ as a function of the lab frame time t for these two assumptions. The region where the dynamics for these two extreme assumptions differ is basically where the dynamics are most uncertain, and corresponds to the range of radii $R_S(E_{jet}) < R < b_2 R_S(E_{iso})$ (i.e. a factor of $f_R \sim \theta_0^{-2/(3-k)} b_2$ in radius), and (lab frame) times $R_S(E_{jet})/c < t < t_{sph,2} \sim \theta_0^{-1} b_2^{(5-k)/2} R_S(E_{iso})/c$ (or a factor of $f_t \sim f_R^{(5-k)/2} \sim \theta_0^{-(5-k)/(3-k)} b_2^{(5-k)/2}$ in time).

Altogether, the ordering of the different radii is

$$R_S(E_{jet}) \sim R_j < R_{NR,1} < R_S(E_{iso}) = R_{NR,2} \quad (6)$$

or

$$1 \sim \frac{R_S(E_{jet})}{R_j} \sim (1 - \ln\theta_0)^{-1} \frac{R_{NR,1}}{R_j} \sim \theta_0^{-2/(3-k)} \frac{R_S(E_{iso})}{R_j}$$

$$= \theta_0^{-2/(3-k)} \frac{R_{NR,2}}{R_j}. \quad (7)$$

3 ANALYTIC RECIPE FOR LATERAL EXPANSION

The 'traditional' basic underlying model assumptions used for the analytic modelling of relativistic jet dynamics during the afterglow phase (e.g. Rhoads 1999; Sari et al. 1999) are (i) a uniform jet within a finite half-opening angle θ_j with an initial value θ_0 that has sharp edges; (ii) the shock front is part of a sphere at any given lab frame

time t; (iii) the outer edge of the jet is expanding sideways mildly relativistically, with $u'_\theta \sim 1$ in the local rest frame of the jet (where quantities are denoted with a prime); and (iv) the jet velocity is always in the radial direction and $\theta_j \ll 1$. Under these assumptions, the jet dynamics are obtained by solving the 1D ordinary differential equations for the conservation of energy and particle number.[2]

The lateral expansion speed in the lab frame (i.e. the rest frame of the central source and the external medium) is $\beta_\theta = u_\theta/\Gamma = u'_\theta/\Gamma$, where $u_\theta = \Gamma\beta_\theta$ is its lateral component of the 4-velocity (which is Lorentz invariant, so that $u'_\theta = u_\theta$), while $u_r = \Gamma\beta_r$ is its radial component. Primed quantities are measured in a frame moving at $\beta_r \hat{\boldsymbol{r}}$ in the radial direction, so that $\beta'_r = 0$ and $\beta' = [1-(\Gamma')^{-2}]^{1/2} = \beta'_\theta$. The usual assumption (Rhoads 1999; Sari et al. 1999) is that $u'_\theta \sim 1$, which corresponds to

$$\beta_\theta \sim \frac{1}{\Gamma}. \tag{8}$$

As is shown in the next section, $\beta_\theta \approx \mathrm{d}\theta_j/\mathrm{d}\ln R$ directly determines the jet lateral expansion rate in the lab frame.

Here we derive a new physically motivated recipe. It relies on the fact that for any shock front, with an arbitrary shape, the local velocity vector of the material just behind the shock front as measured in the rest frame of the upstream fluid ahead of the shock (i.e. the lab frame in our case), $\boldsymbol{\beta}$, is normal to the shock front (i.e. in the direction of the shock normal, $\hat{\boldsymbol{n}}$, at that location; Kumar & Granot 2003), namely

$$\hat{\boldsymbol{\beta}} = \hat{\boldsymbol{n}}. \tag{9}$$

A simple way to understand this result is that as each fluid element passes through the shock, it samples only the local conditions (and is not aware of the large-scale or global shock front geometry), and locally the shock normal is the only preferred direction in the upstream rest frame (e.g. the pressure gradients that accelerate the fluid element are in the $-\hat{\boldsymbol{n}}$ direction and thus accelerate it in the $\hat{\boldsymbol{n}}$ direction). For an axisymmetric shock (with no dependence on the azimuthal angle ϕ), equation (9) immediately implies that the angle α between the shock normal, $\hat{\boldsymbol{n}}$, and the radial direction, $\hat{\boldsymbol{r}}$, which is defined by $\cos\alpha \equiv \hat{\boldsymbol{n}}\cdot\hat{\boldsymbol{r}} = \hat{\boldsymbol{\beta}}\cdot\hat{\boldsymbol{r}}$, satisfies

$$\tan\alpha = \frac{\beta_\theta}{\beta_r} = -\frac{1}{R}\frac{\partial R}{\partial\theta} = -\frac{\partial\ln R}{\partial\theta}, \tag{10}$$

where θ is the polar angle measured from the jet symmetry axis. Since $R \sim \beta ct$, we have $\partial\ln R/\partial\theta \sim \partial\ln\beta/\partial\theta = \Gamma^{-2}\partial\ln u/\partial\theta \sim -1/\Gamma^2\Delta\theta$, where $\Delta\theta$ is the angular scale over which u varies significantly, and we have assumed that u decreases with θ, as is usually expected. Since for $\Gamma \gg 1$ and $\alpha \ll 1$ we also have $\beta_r \approx 1$, equation (10) implies that $\beta_\theta \sim 1/\Gamma^2\Delta\theta$. For a roughly uniform jet of half-opening angle θ_j we have $\Delta\theta \sim \theta_j$, and therefore

$$\beta_\theta \sim \frac{1}{\Gamma^2\Delta\theta} \sim \frac{1}{\Gamma^2\theta_j}, \tag{11}$$

which is our new recipe for lateral expansion.

Equation (11) was first derived in the context of GRBs by Kumar & Granot (2003). Recently it was rederived by Lyutikov (2011), based on an earlier work by Shapiro (1979). Lyutikov (2011) has argued that equation (11) implies a negligible lateral expansion as long as $\Gamma > 1/\sqrt{\theta_j}$, suggesting that with this model one obtains a slow sideways expansion, as seen in the numerical simulations. However, as we show later, this formula results in a slower lateral expansion (compared to the usual recipe, i.e. equation 8) only as long as $\Gamma > 1/\theta_j$ (the standard condition for the onset of significant lateral expansion), but once $\Gamma < 1/\theta_j$ this formula leads to a faster sideways expansion. We also show later that other factors, namely the break down of the ultrarelativistic and small angle approximations, are the main cause for the discrepancy between the existing simple analytic models and the numerical simulations. For completeness we discuss the details of Lyutikov's and Shapiro's work in Appendix A.

4 A SIMPLE RELATIVISTIC MODEL

We turn now to compare the traditional recipe for the lateral expansion speed, $\beta_\theta \sim 1/\Gamma$ (equation 8), with our own new simple recipe, $\beta_\theta \sim 1/\Gamma^2\theta_j$ (equation 11), which was derived in the previous section. These recipes are implemented here within the semi-analytic model for the jet dynamics of Granot (2007). The main results are provided here and we refer the reader to that work for more details on that model. Broadly similar semi-analytic models, with some variations, were used earlier by other authors (e.g. Rhoads 1997; Panaitescu & Mészáros 1999; Rhoads 1999; Sari et al. 1999; Kumar & Panaitescu 2000; Moderski et al. 2000; Oren et al. 2004).

The lateral size of the jet, $R_\perp$, and its radius, $R = R_\parallel$, are related by $R_\perp \approx \theta_j R$. The evolution of $R_\perp$ is governed by

$$\mathrm{d}R_\perp \approx \theta_j \mathrm{d}R + \beta_\theta c\mathrm{d}t \approx (\theta_j + \beta_\theta)\,\mathrm{d}R, \tag{12}$$

and therefore

$$\frac{\mathrm{d}\theta_j}{\mathrm{d}\ln R} \approx \beta_\theta \approx \frac{1}{\Gamma^{1+a}\theta_j^a}, \qquad a = \begin{cases} 1 & (\hat{\boldsymbol{\beta}} = \hat{\boldsymbol{n}}), \\ 0 & (u'_\theta \sim 1), \end{cases} \tag{13}$$

where we have conveniently introduced the parameter a that enables us to analyse these two different recipes together.

The external density is assumed to be a power law in radius,[3] $\rho_{\mathrm{ext}} = AR^{-k}$. The total swept-up (rest) mass, $M(R)$, is accumulated as

$$\frac{\mathrm{d}M}{\mathrm{d}R} \approx 2\pi(\theta_j R)^2\rho_{\mathrm{ext}}(R) = 2\pi AR^{2-k}\theta_j^2(R), \tag{14}$$

where the factor of 2 is since a double-sided jet is assumed. As long as the jet is relativistic, energy conservation takes the form $E_{\mathrm{jet}} \approx \Gamma^2 Mc^2$, which implies that $M\mathrm{d}(\Gamma^2) = -\Gamma^2\mathrm{d}M$, and

$$\frac{\mathrm{d}\Gamma}{\mathrm{d}R} = -\frac{\Gamma}{2M}\frac{\mathrm{d}M}{\mathrm{d}R} = -\pi AR^{2-k}\theta_j^2(R)\frac{\Gamma(R)}{M(R)}. \tag{15}$$

One can numerically integrate equations (13)–(15), thus obtaining $\theta_j(R)$, $M(R)$ and $\Gamma(R)$. Alternatively, one can use the relation $E_{\mathrm{jet}} \approx \Gamma^2 Mc^2$ (energy conservation) which reduces the number of free variables to two, and solve equations (13) and (15). Changing to normalized dimensionless variables $\theta \equiv \theta_j/\theta_0$, $\gamma \equiv \Gamma\theta_0$ and $r \equiv [(3-k)/2]^{1/(3-k)}R/R_j$ gives

$$\frac{\mathrm{d}\theta}{\mathrm{d}r} = r^{-1}\gamma^{-1-a}(r)\theta^{-1}(r), \tag{16}$$

---

[2] For the adiabatic energy conserving evolution considered here, the equation for momentum conservation is trivial in spherical geometry, and does not constrain the dynamics. For a narrow ($\theta_j \ll 1$) highly relativistic ($\Gamma \gg 1$) jet, the equation for the conservation of linear momentum in the direction of the jet symmetry axis is almost identical to the energy conservation equation. When the jet becomes subrelativistic the conservation of energy and linear momentum force it to approach spherical symmetry, and once it becomes quasi-spherical then again the momentum conservation equation becomes irrelevant.

[3] We consider here and throughout this review only $k < 3$ for which the shock Lorentz factor decreases with radius for a spherical adiabatic blast wave during the self-similar stage of its evolution (Blandford & McKee 1976).

$$\frac{d\gamma}{dr} = -r^{2-k}\,\gamma^3(r)\,\theta^2(r), \tag{17}$$

where the initial conditions at some small radius $r_0 \ll 1$ (just after the deceleration radius) are

$$\theta(r_0) = 1, \qquad \gamma(r_0) = \sqrt{\frac{3-k}{2}}\,r_0^{-(3-k)/2}. \tag{18}$$

Note that by definition, $\gamma\theta = \Gamma\theta_j$. Equations (16) and (17) imply

$$\frac{d(\gamma\theta)}{dr} = \frac{1}{r(\gamma\theta)^a} - r^{2-k}(\gamma\theta)^3 = \frac{1 - r^{3-k}(\gamma\theta)^{3+a}}{r(\gamma\theta)^a}. \tag{19}$$

For $r \ll 1$ the second term on the right-hand side of equation (19) dominates, implying $(\gamma\theta)^2 \approx [(3-k)/2]r^{k-3}$, which is consistent with equation (18). This suggests that the two terms become comparable at $r \approx r_c$ that is given by

$$r_c = \left(\frac{3-k}{2}\right)^{(3+a)/[(1+a)(3-k)]}. \tag{20}$$

While $r_c > 1$ for $k < 1$, it can reach very low values ($r_c \ll 1$) as k approaches 3. We are interested here mainly in $k \geqslant 2$, for which $r_c \sim 1$ still approximately holds. We do note, however, that the lower values of r_c for higher values of k result in an earlier onset of significant lateral expansion for such higher k-values. Now let us examine what happens at $r \gg r_c \sim 1$. If we assume that the first term becomes dominant, then equation (19) would imply $\gamma\theta \approx [(1+a)\ln r]^{1/(1+a)}$, which in turn implies that the second term would be dominant (since $(\gamma\theta)^{3+a}r^{3-k} \approx [(1+a)\ln r]^{(3+a)/(1+a)}r^{3-k} \gg 1$), rendering the original assumption inconsistent. The same applies if the opposite assumption is made, that the second term is dominant (in this case $\gamma\theta \approx \sqrt{\frac{3-k}{2}}r^{(k-3)/2}$ which implies that the first term would be dominant, $(\gamma\theta)^{3+a}r^{3-k} \approx [(3-k)/2]^{(3+a)/2}r^{(k-3)(1+a)/2} \ll 1$). This implies that the two terms must remain comparable, implying $\gamma\theta \sim r^{(k-3)/(3+a)}$. A similar conclusion can be reached by taking the ratio of equations (16) and (17) which implies that

$$d(\theta^{3+a}) = r^{k-3}d(\gamma^{-3-a}). \tag{21}$$

A more careful examination shows that they must cancel each other to leading order, and the first two leading terms for $r \gg 1$ are given by

$$\gamma\theta \approx r^{(k-3)/(3+a)} + \frac{3-k}{(3+a)^2}\,r^{(k-3)(2+a)/(3+a)}. \tag{22}$$

Substituting equation (22) into equations (16) and (17) yields

$$\frac{d\ln\theta}{d\ln r} \approx r^{(3-k)(1+a)/(3+a)} - \frac{(3-k)(1+a)}{(3+a)^2}, \tag{23}$$

$$\frac{d\ln\gamma}{d\ln r} \approx -r^{(3-k)(1+a)/(3+a)} - \frac{2(3-k)}{(3+a)^2} \tag{24}$$

and

$$\theta \approx b\,r^{-(3-k)(1+a)/(3+a)^2}\exp\left[\frac{(3+a)}{(3-k)(1+a)}\,r^{(3-k)(1+a)/(3+a)}\right], \tag{25}$$

$$\gamma \approx \frac{1}{b}\,r^{-2(3-k)/(3+a)^2}\exp\left[-\frac{(3+a)}{(3-k)(1+a)}\,r^{(3-k)(1+a)/(3+a)}\right], \tag{26}$$

where the normalization coefficient b is determined numerically. For $r \ll 1$ we have

$$\gamma\theta \approx \sqrt{\frac{3-k}{2}}\,r^{(k-3)/2} + \left(\frac{3-k}{2}\right)^{(-2-a)/2}\frac{r^{a(3-k)/2}}{(3+a)}. \tag{27}$$

Fig. 2 shows the results of our model in terms of the normalized jet half-opening angle $\theta = \theta_j/\theta_0$ and Lorentz factor $\gamma = \Gamma\theta_0$ (as well as their product, $\gamma\theta = \Gamma\theta_j$) as a function of the normalized radius $r = [(3-k)/2]^{1/(3-k)}R/R_j$. The results are shown both for a uniform external medium ($k = 0$), which is the main focus of this work, as well as for a stellar wind ($k = 2$; this is included mainly for completeness and is only briefly discussed in Section 7). The dynamical range in this figure is unrealistically large, and it is shown mainly in order to demonstrate the properties of this solution, and show how well our analytic approximation for $r > 1$ works (the dashed green lines in the middle and bottom panels, which are practically on top of the numerical results). The excellent agreement between our semi-analytic results (the numerical solution of equations 16 and 17) and analytic formulae (equations 25 and 26) shows that our analytic results (including equations 22 and 27) can be safely used in order to analyse the result of this model. This good agreement was also used in order to find the exact values of the numerical coefficient b that determines the normalization for θ and γ, which were found to be $b(k = 0, a = 0) \approx b(k = 0, a = 1) \approx 0.60$, $b(k = 2, a = 0) \approx 0.395$ and $b(k = 2, a = 1) \approx 0.45$. Our new recipe for the lateral expansion speed (equation 11) results in a slower initial lateral expansion compared to the old recipe at $r \ll 1$, where $\Gamma\theta_j = \gamma\theta \gg 1$. However, at larger radii, $r \gtrsim 1$, where $\Gamma\theta_j < 1$, it results in a faster lateral expansion.

Fig. 3 shows similar results for a uniform external medium ($k = 0$) and for three different values of the initial jet half-opening angle, $\theta_0 = 0.05, 0.1$ and 0.2. Since the dynamical equations (equations 16 and 17) involve only the normalized variables θ, γ and r, and the initial conditions (equation 18) for θ and γ depend only on the initial normalized radius r_0, the lines for these normalized variables in the top two panels for the different θ_0 values exactly coincide.[4] The two bottom panels show the unnormalized quantities θ_j and Γ for our three values of θ_0. In the bottom panel we have added for comparison the Sedov radius, $R_S(E_{iso})$, for a spherical flow with the same isotropic equivalent energy the jet started with. We define R_{NR} for our model as the radius where formally $\Gamma = 1$ (at which point this model clearly breaks down). Fig. 4 is similar to Fig. 3, but the jet radius R is normalized by the radius $R_S(E_{iso}) = \theta_0^{-2/(3-k)}R_j$ instead of $[(3-k)/2]^{-1/(3-k)}R_j = [(3-k)/4]^{-1/(3-k)}R_S(E_{jet})$.

Fig. 5 shows R_{NR}/R_j and $\theta_j(R_{NR})$ as a function of θ_0. It can be seen that R_{NR} depends on θ_0 only logarithmically (as can also be seen from equation 26), while $R_S(E_{iso})/R_j = \theta_0^{-2/(3-k)}$ is simply a power of θ_0. It is also evident that $\theta_j(R_{NR}) < 1$ for $\theta_0 \ll 1$, and its value increases with θ_0 (while $\theta_j(R_{NR})/\theta_0$ decreases with θ_0). This can also be seen from equation (22), using the leading-order term in r and the definition $\Gamma(r_{NR}) = 1$, which imply that $\theta_j(r_{NR}) = r_{NR}^{-(3-k)/(3+a)}$, while r_{NR} (or R_{NR}) decreases (logarithmically) with θ_0. For $k = 2$ the jet becomes non-relativistic and the model breaks down at smaller values of $r = [(3-k)/2]^{1/(3-k)}R/R_j$ compared to $k = 0$, which is consistent with the fact that the jet also starts to spread sideways significantly at smaller values of r, of the order of $r_c \approx [(3-k)/2]^{(3+a)/[(1+a)(3-k)]}$. However, we are primarily interested here in $k = 0$.

The model breaks down when Γ drops to 1 (or even slightly earlier). As can be seen from Figs 2–4, it breaks down earlier for larger θ_0 values, and its region of validity (especially at $R \gtrsim R_j$) decreases as θ_0 increases. In particular, for the value of $\theta_0 = 0.2$, which was most widely used so far in numerical simulations

---

[4] This is since the same value of $r_0 = 0.4$ was used, but in the limit $r_0 \ll 1$ the dependence of the solution on r_0 goes away at $r \gg r_0$.
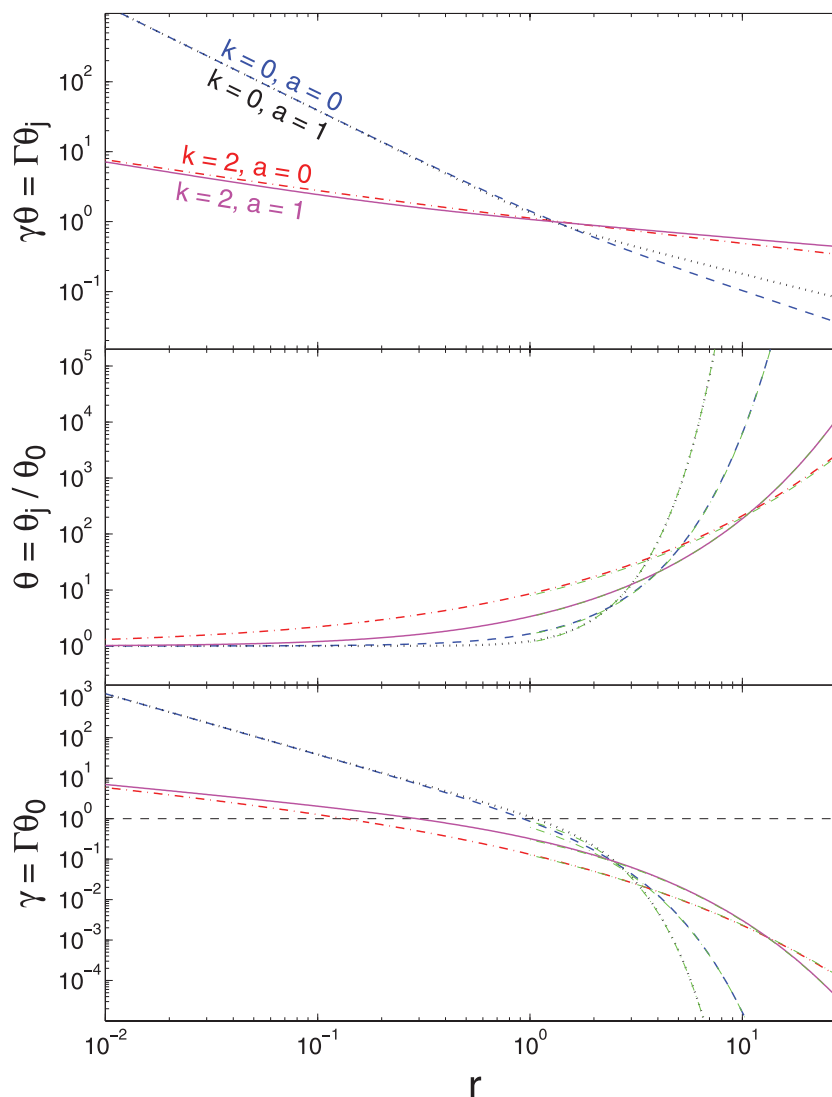
Figure 2. The jet dynamics according to our relativistic analytic model (see text in Section 4 for details), for either a uniform ($k = 0$) or a wind-like, stratified ($k = 2$) external density profile, and for either the old ($a = 0$) or our new ($a = 1$) recipe for the jet lateral expansion speed. The dynamical range in this figure is unrealistically large, and it is shown mainly in order to demonstrate the properties of this solution, and show how well our analytic approximation for $r > 1$ works (the dashed green lines in the middle and bottom panels, which are practically on top of the numerical results).

(Granot et al. 2001; Zhang & MacFadyen 2009; van Eerten et al. 2010), while an even larger value of $\theta_0 = 20° \approx 0.35$ rad was used in some works (Meliani & Keppens 2010; van Eerten et al. 2011a), this dynamical range is very narrow, and the asymptotic exponential growth of θ_j with R is not reached before the model breaks down at $\Gamma \gtrsim 1.5-2$ or $\theta_j \lesssim 0.5-1$. Even for $\theta_0 = 0.05$, which was used in the most recent simulations (van Eerten & MacFadyen 2011; Wygoda et al. 2011) and is at the low end of the values inferred from afterglow observations, the asymptotic exponential regime is only barely reached before the model breaks down (in agreement with the conclusions of Wygoda et al. 2011). Note that in this (limited) region of validity of this semi-analytic model, our new recipe might still result in smaller or comparable values of $\theta(r)$ (i.e. of θ_j for a fixed θ_0, at a given radius for a fixed E_{jet}) compared to the old recipe. The discussion about when this model breaks down is expanded in Section 6, where we compare the analytic models to numerical simulations. Because of this important limitation of our

relativistic analytic model, in the next section we generalize it so that it would not break down when the jet becomes subrelativistic or wide.

5 GENERALIZED MODELS VALID FOR ARBITRARY Γ AND θ_j

In order to avoid the breakdown of the model at small Lorentz factors Γ or large jet half-opening angles θ_j, we construct here simple generalizations of the analytic model studied in the previous section, which do not require the jet to be very narrow ($\theta_j \ll 1$) or highly relativistic ($u \approx \Gamma \gg 1$). Two variants are introduced, named the trumpet model (in Section 5.1) and the conical model (in Section 5.2), according to the shape of the region from which the external medium is assumed to have been swept up by the jet (before it becomes spherical).
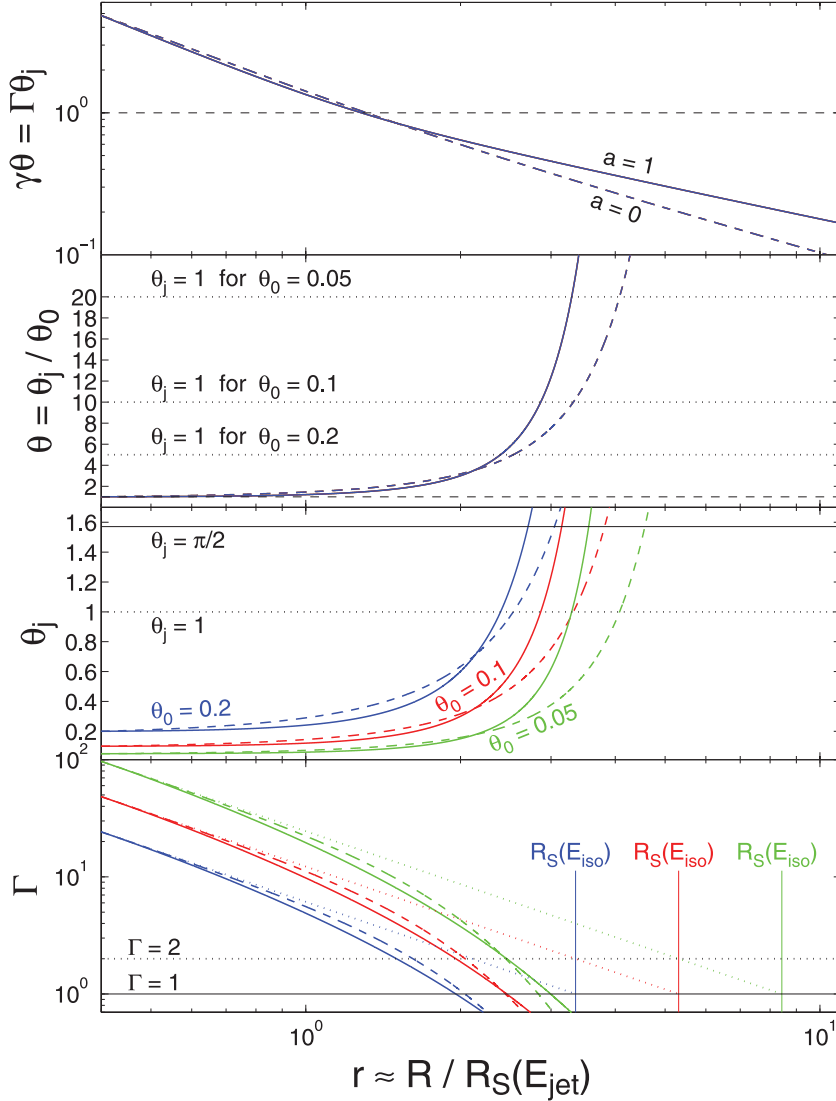
Figure 3. Similar to Fig. 2 but only for a uniform external density ($k = 0$) and for three different values of the initial jet half-opening angle: $\theta_0 = 0.05$ (green), $\theta_0 = 0.1$ (red) and $\theta_0 = 0.2$ (blue). The old ($a = 0$) and new ($a = 1$) recipes for the jet lateral expansion are sown by dashed and solid lines, respectively. In the top two panels the lines for different θ_0 and the same a values coincide (see text for details). The values of $R_{\rm S}(E_{\rm iso})$ are indicated in the bottom panel for reference.

The rate at which the jet half-opening angle, $\theta_{\rm j}$, increases depends on the lateral velocity at the edge of the jet, β_θ, as $d\theta_{\rm j} = \beta_\theta c\, dt/R = (\beta_\theta/\beta_r)dR/R$, or

$$\frac{d\theta_{\rm j}}{d\ln R} = \frac{\beta_\theta}{\beta_r}. \qquad (28)$$

A crude approximation for the comoving 4-velocity of the lateral expansion (u'_θ), which would roughly correspond to the sound speed both in the relativistic and in the Newtonian regimes, is $u'_\theta \sim \beta = u(1 + u^2)^{-1/2}$. This would modify the traditional recipe to $\beta_\theta = u'_\theta/\Gamma \sim \beta/\Gamma = u/(1 + u^2)$ or $\beta_\theta/\beta_r \sim \beta_\theta/\beta \sim 1/\Gamma = (1 + u^2)^{-1/2}$. In our recipe,[5] $\beta_\theta/\beta_r = -\partial \ln R/\partial\theta \sim -\partial \ln \beta/\partial\theta \sim$

$-\Gamma^{-2}\partial \ln u/\partial\theta \sim 1/\Gamma^2 \Delta\theta \sim 1/\Gamma^2\theta_{\rm j} = 1/[(1+u^2)\theta_{\rm j}]$. Therefore, just as before, we still have

$$\frac{d\theta_{\rm j}}{d\ln R} = \frac{\beta_\theta}{\beta_r} \approx \frac{1}{\Gamma^{1+a}\theta_{\rm j}^a}, \qquad a = \begin{cases} 1 & (\hat{\boldsymbol{\beta}} = \hat{\boldsymbol{n}}), \\ 0 & (u'_\theta \sim 1). \end{cases} \qquad (29)$$

5.1 The 'trumpet model'

In this model we follow the usual assumption that the external rest mass is swept up by a working area consisting of the part of an expanding sphere of radius R within a half-opening angle $\theta_{\rm j}(R)$. Thus, the total swept-up (rest) mass, $M(R)$, for a double-sided jet is accumulated as

$$\frac{dM}{dR} \approx [1 - \cos\theta_{\rm j}(R)]4\pi R^2 \rho_{\rm ext}(R) = [1 - \cos\theta_{\rm j}(R)]4\pi A R^{2-k}. \qquad (30)$$

---

[5] Note that we use $\partial \ln u/\partial\theta = u^{-1}\partial u/\partial\theta \sim -1/\Delta\theta$ since the 4-velocity u, unlike β or Γ, generally varies significantly with θ both in the relativistic and in the Newtonian regimes, so that $\partial u/\partial\theta \sim -u/\Delta\theta$ in both regimes, while $\partial\Gamma/\partial\theta \sim -\Gamma/\Delta\theta$ only in the relativistic regime and $\partial\beta/\partial\theta \sim -\beta/\Delta\theta$ only in the Newtonian regime.
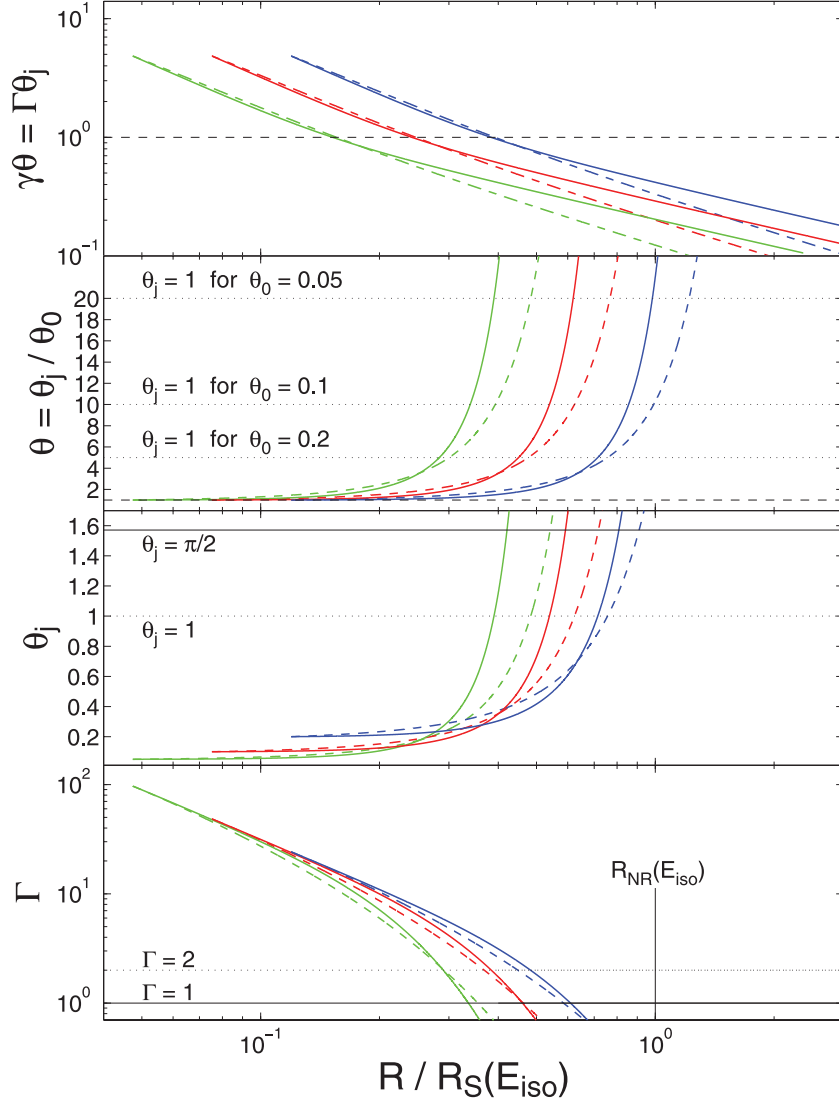
Figure 4. Similar to Fig. 3 but shown as a function of the jet radius R normalized by $R_S(E_{iso}) = R_j \theta_0^{-2/(3-k)}$ instead of $[(3-k)/2]^{-1/(3-k)} R_j = [(3-k)/4]^{-1/(3-k)} R_S(E_{jet})$, where $E_{iso} \approx E_{jet} 2/\theta_0^2$ is the isotropic equivalent energy in the jet, while E_{jet} is its true energy.

Energy conservation takes the approximate form $E_{jet} \approx u^2 M c^2$, implying $M\mathrm{d}(u^2) = -u^2 \mathrm{d}M$, and

$$\frac{\mathrm{d}u}{\mathrm{d}R} = -\frac{u}{2M}\frac{\mathrm{d}M}{\mathrm{d}R} = -\frac{2\pi A c^2}{E_{jet}} R^{2-k}[1 - \cos\theta_j(R)]u^3(R). \quad (31)$$

Thus, in terms of $r = [(3-k)/2]^{1/(3-k)} R/R_j$, we have

$$\frac{\mathrm{d}\theta_j}{\mathrm{d}\ln r} \approx \frac{1}{(1+u^2)^{(1+a)/2}\theta_j^a}, \quad \frac{\mathrm{d}u}{\mathrm{d}r} = -r^{2-k}u^3(r)2[1 - \cos\theta_j(r)], \quad (32)$$

where the initial conditions at some small radius $R_0 \ll R_S(E_{jet}) \sim R_j$ (just after the deceleration radius), corresponding to r_0, are given by

$$\theta_j(r_0) = \theta_0, \quad u(r_0) = \sqrt{\frac{3-k}{4(1-\cos\theta_0)}} r_0^{-(3-k)/2}. \quad (33)$$

5.2 The 'conical model'

Here we note that the usual assumption that leads to equation (30) neglects the external matter at the sides of the jet. Because of this, when eventually θ_j reaches $\pi/2$ at R_{sph} and is thus assumed to be fully spherical, the amount of swept-up external rest mass at R_{sph} calculated according to equation (30) will be significantly smaller than that originally within a sphere of the same radius. Therefore, here in the conical model we adopt an alternative approach of using for the rest mass of the swept-up matter, originally within a cone of half-opening angle θ_j,

$$M(R) \approx [1 - \cos\theta_j(R)]\frac{4\pi}{(3-k)}A R^{3-k}. \quad (34)$$

This still has the drawback of assigning the same Lorentz factor to all of the swept-up external matter, even though that at the sides of the jet should have a significantly smaller 4-velocity than that near the head of the jet. Using a slightly different normalized radius, $r_S = R/R_S(E_{jet}) = 2^{1/(3-k)}R/R_j = [4/(3-k)]^{1/(3-k)}r$, energy conservation
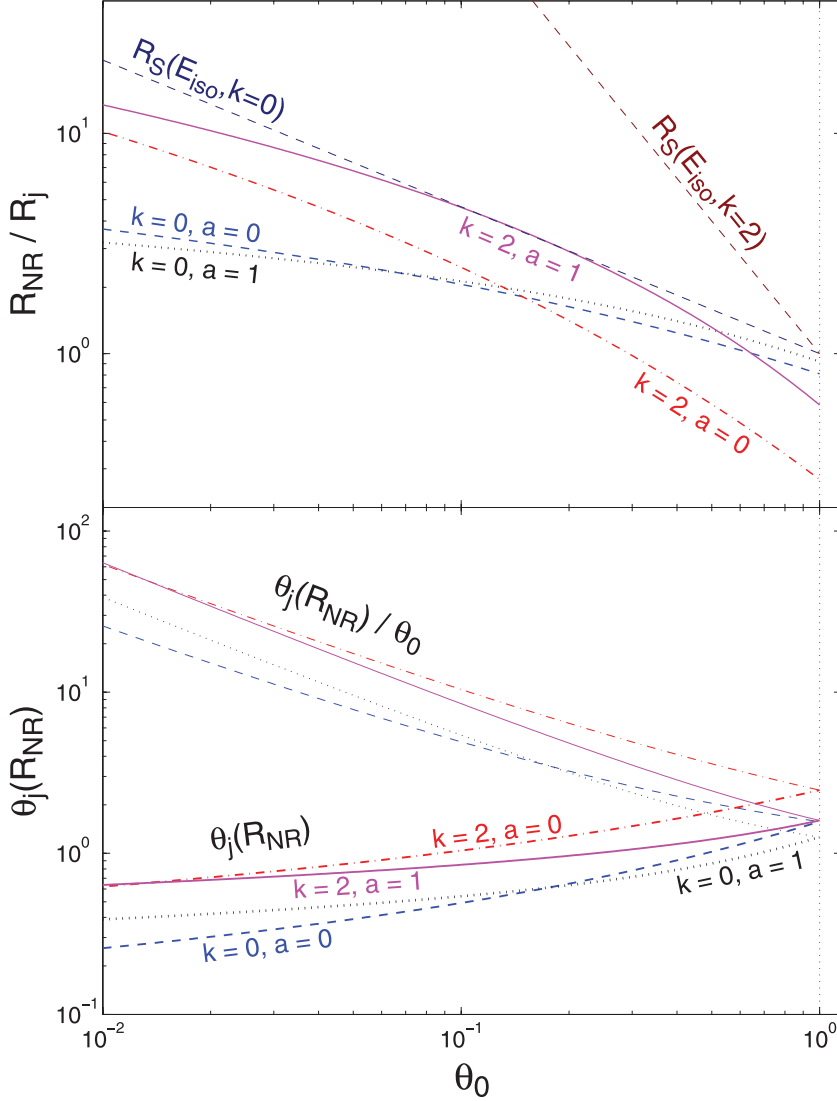
Figure 5. Upper panel: the non-relativistic transition radius for our analytic relativistic model, R_{NR}, defined by $\Gamma(R_{NR}) = 1$, normalized by R_j, as a function of θ_0. For comparison, $R_S(E_{iso})$ is also shown; the two radii, R_{NR} and $R_S(E_{iso})$, become similar at $\theta_0 \sim 1$ but are very different for $\theta_0 \ll 1$. Lower panel: the value of the jet half-opening angle, θ_j, at R_{NR}, where our simple analytic relativistic model breaks down.

($E_{jet} \approx u^2 Mc^2$) and equation (29) imply

$$u(r_S) = \frac{r_S^{-(3-k)/2}}{\sqrt{1 - \cos\theta_j(r_S)}},$$

$$\frac{d\theta_j}{d\ln r_S} \approx \frac{1}{[1 + r_S^{k-3}(1 - \cos\theta_j)^{-1}]^{(1+a)/2}\theta_j^a}, \tag{35}$$

where the initial conditions at some small radius $R_0 \ll R_{NR,sph}(E) \sim R_j$, corresponding to $r_{S,0}$, are given by

$$\theta_j(r_{S,0}) = \theta_0, \qquad u(r_{S,0}) = \frac{r_{S,0}^{-(3-k)/2}}{\sqrt{1 - \cos\theta_0}}. \tag{36}$$

5.3 Results for the generalized models

Figs 6–8 depict a comparison of these two models with the relativistic model. All three models agree at early times, while the jet is still highly relativistic, narrow and hardly expanded sideways. The approximations of our relativistic model hold well at this stage, and

the difference in the swept-up mass between the trumpet and conical models is still very small. At later times, however, the three models show a different behaviour. The main effect of the relaxation of the small θ and ultrarelativistic approximations is that for typical values of $\theta_0 \gtrsim 0.05$ the region of exponential growth of θ_j with R largely disappears, and is replaced by a much slower, quasi-logarithmic growth. This can most clearly be seen by comparing the results of the relativistic model (from Section 4; solid lines in Figs 6 and 8, and green, red or blue lines in Fig. 7) and the trumpet model (from Section 5.1; dot–dashed lines in Figs 6 and 8, and black, magenta or cyan lines in Fig. 7). These two models share the same assumption on the accumulation of the swept-up external medium, and differ only by relaxing in the trumpet model the requirements of $\Gamma \gg 1$ and $\theta_j \ll 1$. The results of these two models are very close at early times while $\Gamma \gg 1$, but diverge as Γ becomes more modest and the simple relativistic model reaches the exponential regime. This can also be seen in Fig. 8 through the fact that $\theta_j(r)$ for the two models start diverging when θ_j becomes modest and the small angle approximation breaks down.
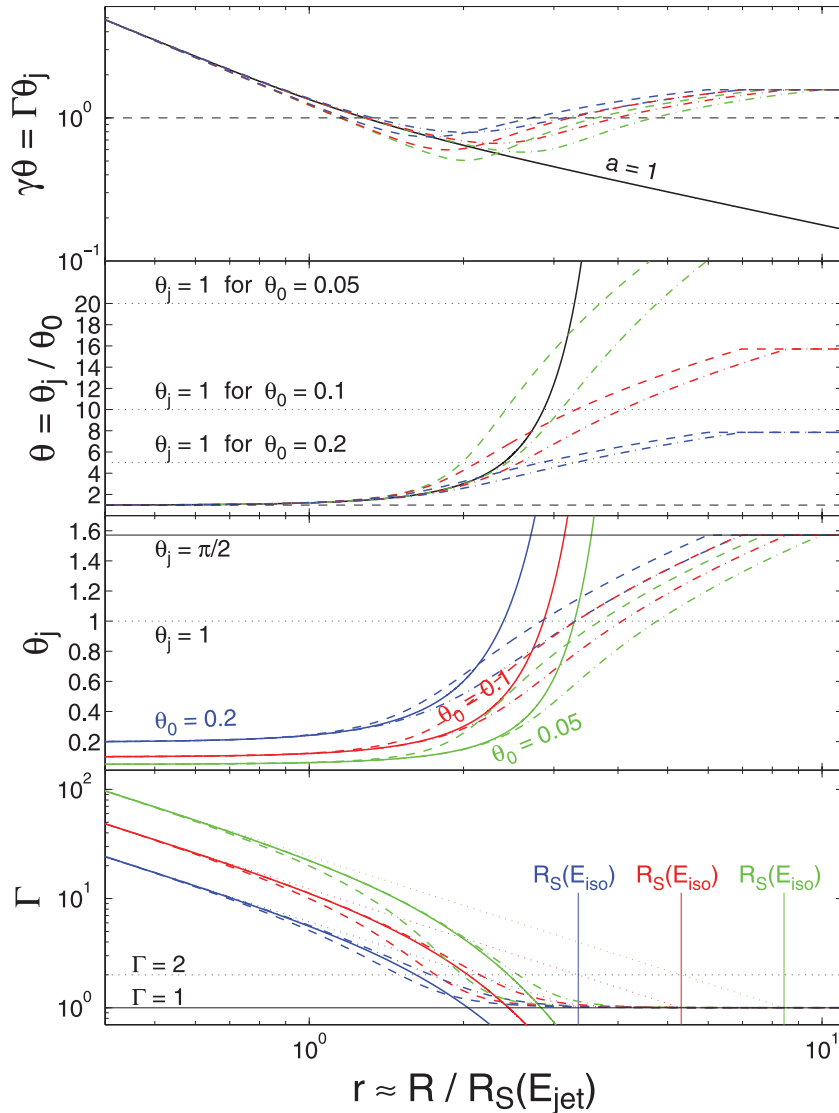
Figure 6. Comparison between our relativistic (solid lines), trumpet (dot–dashed lines) and conical (dashed lines) models, where all models use our new recipe for the lateral spreading of the jet ($a = 1$), and for a uniform external medium ($k = 0$). Results are shown for three different values of the jet initial half-opening angle: $\theta_0 = 0.05$ (in green), $\theta_0 = 0.1$ (in red) and $\theta_0 = 0.2$ (in blue). For reference we also indicate the values of $\Gamma\theta_j = 1$ in the top panel, some relevant values of θ_j in the two middle panels, as well as the values of $R_S(E_{\rm iso})$ and $\Gamma = 1, 2$ in the bottom panel.

The main difference between the trumpet and conical models is that for the conical model the swept-up mass at a given radius R is larger than for the trumpet model, resulting in a smaller Γ and therefore also a larger θ_j, i.e. a faster evolution of θ_j and Γ with R. Since the larger swept-up mass comes from the sides of the jet, it becomes important only once the jet starts expanding sideways significantly, which occurs at r_c (see equation 20). This can be clearly seen in Fig. 8, where the dot–dashed (or solid, which practically coincide at early times) and dashed lines, for the trumpet (or relativistic) and conical models, respectively, start diverging near r_c. Note that this remains valid for all k-values, while r_c decreases with k. Fig. 8 also shows that for sufficiently small values of θ_0, roughly $\theta_0 \ll 0.05$ for $k = 0$ and even somewhat smaller θ_0 values for larger k values, there is still a phase of quasi-exponential lateral expansion for $r_c \lesssim r \lesssim r(\theta_j \sim 10^{-0.5})$ or $1.5\theta_0 \lesssim \theta_j \lesssim 10^{-0.5}$. For such extremely small values of θ_0, the difference between the conical and trumpet models becomes large during the exponential sideways expansion phase, where the lateral

expansion is faster in the conical model. We note, however, that such extremely narrow initial jet half-opening angles are below the smallest values that have so far been reliably inferred from GRB afterglow modelling, so that they might not be very relevant in practice.

Figs 9 and 10 show the jet dynamics according to our different analytic models, for $\theta_0 = 0.1$. It can be seen that the differences between the various models are rather small until the point where our relativistic model breaks down. The behaviour of the jet radius ($R = R_{\parallel}$) and lateral size ($R_{\perp}$) as a function of the lab frame time (t) shows a lot of similarities to the analytic expectations (compare the bottom panel of Fig. 9 to Fig. 1). This, again, demonstrates that our new recipe for the lateral spreading of the jet results in slower lateral expansion compared to the old recipe (and is closer to assumption 2 of no lateral spreading – dashed red lines in Fig. 1) at early times when $\Gamma > \theta_j$ but faster lateral expansion at late times when $\Gamma < \theta_j$ (i.e. closer to assumption 1 of fast lateral spreading – solid blue lines in Fig. 1).
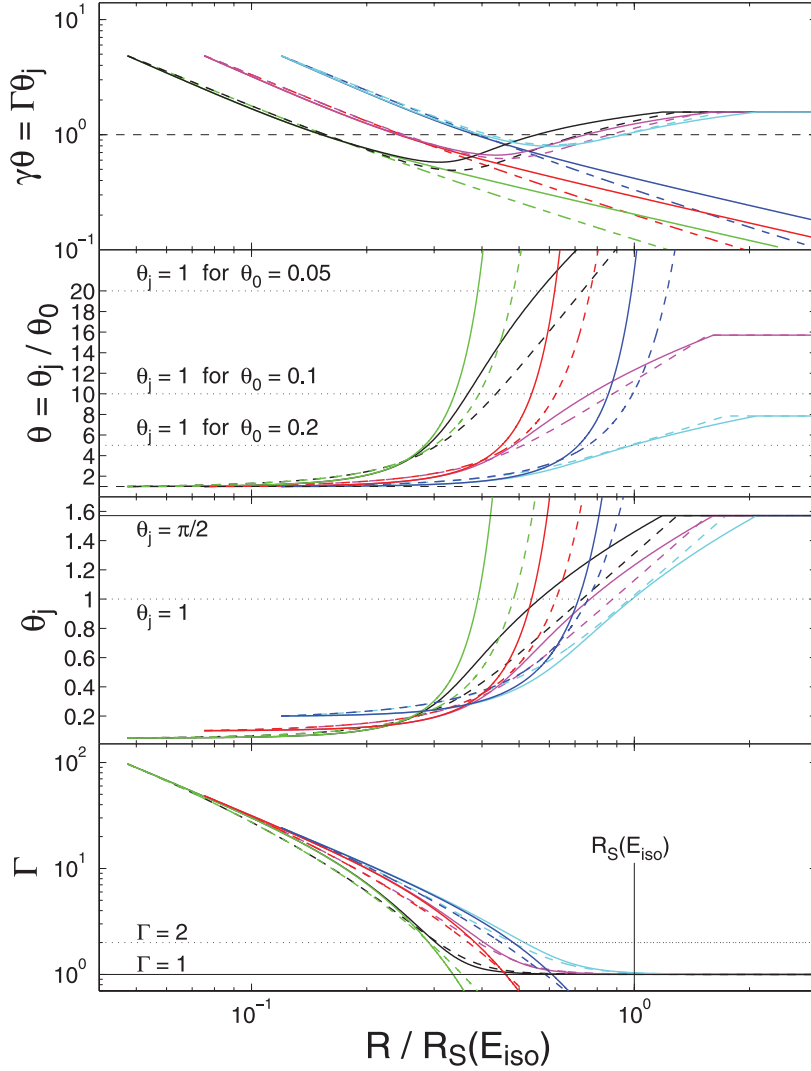
Figure 7. Similar to Fig. 6 but shown only (1) for our relativistic model (green, red and blue lines for $\theta_0 = 0.05$, 0.1 and 0.2, respectively) and trumpet model (black, magenta and cyan lines for $\theta_0 = 0.05$, 0.1 and 0.2, respectively), (2) for both the old recipe ($a = 0$; dashed lines) and our new recipe ($a = 1$; solid lines) for the jet lateral expansion and (3) as a function of the jet radius R normalized by $R_S(E_{iso}) = R_j \theta_0^{-2/(3-k)}$ instead of $[(3 - k)/2]^{-1/(3-k)} R_j = [(3 - k)/4]^{-1/(3-k)} R_S(E_{jet})$.

6 COMPARISON WITH NUMERICAL SIMULATIONS

We turn now to a comparison of our analytic models with the results of full 2D special relativistic hydrodynamic simulations. To do so, one needs first to define which quantities should be compared. This, however, is not unique and can be done in different ways. For the 4-velocity, u, and as one (out of a few) reference value for the jet half-opening angle, θ_j, we use the weighted mean over the energy E in the lab frame (excluding rest energy) of u and θ, respectively,

$$\langle u \rangle_E = \frac{\int dE\, u}{\int dE}, \qquad \langle \theta \rangle_E = \frac{\int dE\, \theta}{\int dE}. \qquad (37)$$

For the jet radius (or parallel size, $R_\parallel = R$) and lateral size ($R_\perp$), we use

$$\langle R_\parallel \rangle = \langle z \rangle_E = \frac{\int dE\, z}{\int dE},$$

$$\langle R_\perp \rangle = \langle x \rangle_E = \langle y \rangle_E = \frac{2}{\pi} \langle r_{cyl} \rangle_E = \frac{2}{\pi} \frac{\int dE\, r_{cyl}}{\int dE}. \qquad (38)$$

These averages reduce to $R_\parallel = R_\perp$ (or $\langle R_\parallel \rangle = \langle R_\perp \rangle$) for a spherical flow.

In order to perform a proper comparison to our analytic models, we need to calculate similar averages for our jet, which at any given time is the part of a thin spherical shell within a cone of half-opening angle θ_j. Thus, the radial integration drops out and we are left only with an integral over μ between $\mu_j = \cos\theta_j$ and 1,
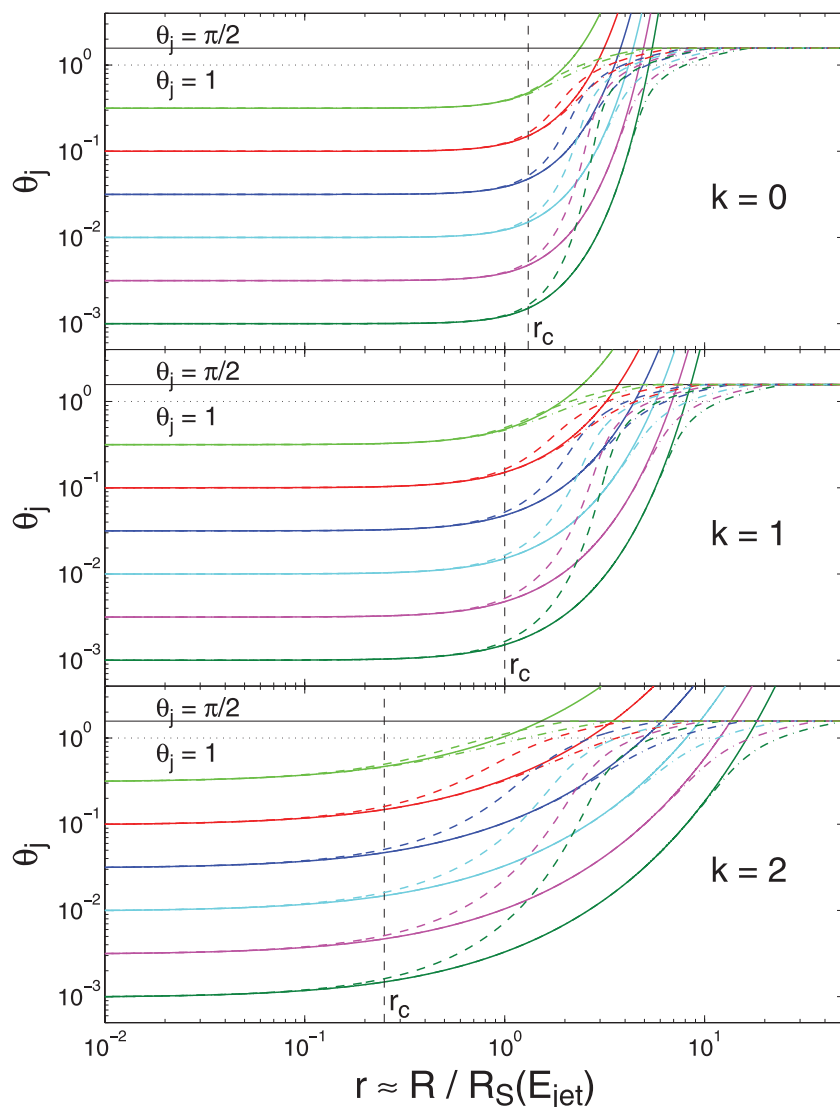
$$\frac{R_\parallel}{R} = \frac{\int_{\mu_j}^1 d\mu\, \mu}{\int_{\mu_j}^1 d\mu} = \frac{\sin^2\theta_j}{2(1 - \cos\theta_j)},$$

$$\frac{R_\perp}{R} = \frac{2}{\pi} \frac{\int_{\mu_j}^1 d\mu\, \sqrt{1 - \mu^2}}{\int_{\mu_j}^1 d\mu} = \frac{2\theta_j - \sin(2\theta_j)}{2\pi(1 - \cos\theta_j)}. \qquad (39)$$

We can see that $R_\parallel = R_\perp$ for $\theta_j = \pi/2$, as it should.

Similarly, one can calculate $\langle \theta \rangle_E$ as a proxy for θ_j in our models,

$$\langle \theta \rangle_E = \frac{\int_{\mu_j}^1 d\mu\, \arccos(\mu)}{\int_{\mu_j}^1 d\mu} = \frac{\int_0^{\theta_j} d\theta\, \theta \sin\theta}{1 - \cos\theta_j} = \frac{\sin\theta_j - \theta_j \cos\theta_j}{1 - \cos\theta_j}. \qquad (40)$$

Figure 8. Comparison between our relativistic (solid lines), trumpet (dot–dashed lines) and conical (dashed lines) models in terms of the evolution of the jet half-opening angle θ_j with the normalized radius r, for $k = 0, 1$ and 2 (top to bottom panels), where all models use our new recipe for the lateral spreading of the jet ($a = 1$). Results are shown for $\log_{10}(\theta_0) = -3, -2.5, \ldots, -0.5$ (using different colours), while the values of $\theta_0 = 1$, $\pi/2$ and the critical radius r_c (given by equation 20, where the lateral spreading is expected to become significant) are shown for reference.

This shows that $\langle\theta\rangle_E \approx (2/3)\theta_j$ for $\theta_j \ll 1$, while $\langle\theta\rangle_E = 1$ for $\theta_j = \pi/2$ (which is the value for any spherical flow, also one with a radial profile) and $(2/3)\theta_j < \langle\theta\rangle_E < (2/\pi)\theta_j$ for $0 < \theta_j < \pi/2$. One can also calculate the angle out to which a fraction f of the energy is contained (or the energy $100f$ percentile),

$$\theta_f = \arccos[1 - f(1 - \cos\theta_j)], \qquad (41)$$

and compare it to the corresponding value from the numerical simulations.

Figs 11 and 12 show a comparison (for $k = 0$ and $\theta_0 = 0.2$) between the results of our analytic models and of 2D special relativistic hydrodynamic simulations (from De Colle et al. 2011a,b), when quantifying all of them as discussed above. As can be seen from Fig. 11, our models provide a reasonable overall description of the full hydrodynamic simulations, and thus appear to catch the basic underlying physics, despite their obvious simplicity.

Fig. 12 shows three different ways of quantifying the jet half-opening angle, namely the weighted mean over the energy, $\langle\theta\rangle_E$ (bottom panel), and two different energy percentiles, $\theta_{0.75}$ (middle panel) and $\theta_{0.95}$ (top panel), i.e. the values of θ up to which 75 and 95 per cent of the energy, respectively, is contained. It can be seen that $\theta_{0.95}$ provides the best match between our analytic model and the numerical simulations. For $\theta_{0.75}$ or $\langle\theta\rangle_E$ the match is not as good (though even then the difference is not very large). This might be attributed to the fact that our analytic models assume a uniform energy per solid angle, $\epsilon = dE/d\Omega$, within the jet opening angle ($\theta < \theta_j$), while in practice (or in the numerical simulations) it drops towards the outer edge of the jet. The drop in ϵ from the jet axis towards its edge causes smaller values of both $\langle\theta\rangle_E$ and θ_f for the lower energy percentiles (or f-values) relative to a uniform jet with the same θ_f for a large energy percentile (or f-value; e.g. $f = 0.95$ in our case). The results for our new recipe for the jet sideways expansion are somewhat closer to the numerical simulations compared to the usual recipe for
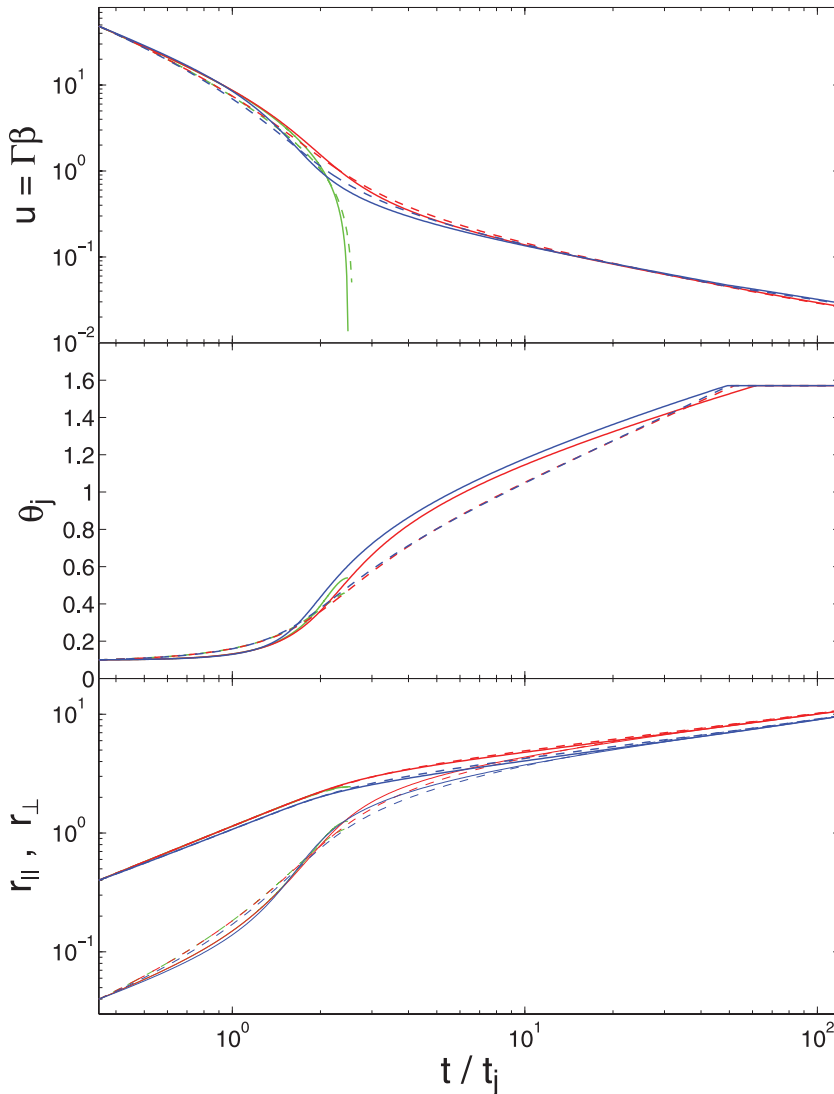
Figure 9. The jet dynamics according to our different analytic models, for $\theta_0 = 0.1$ and $k = 0$. We show the jet 4-velocity, u (upper panel), half-opening angle, θ_j (middle panel), as well as its normalized radius $r_\parallel = r$ and lateral size $r_\perp = r\sin\theta_j$ (bottom panel), as a function of the normalized lab frame time, t/t_j, for our relativistic (green lines; until it breaks down at $\Gamma \approx 1$), trumpet (red lines) and conical (blue lines) models. The solid and dashed lines are, respectively, for our new recipe ($a = 1$; equation 9) and the old recipe ($a = 0$; equation 8) for the jet lateral expansion.

$\langle\theta\rangle_E$ and $\theta_{0.75}$, while the usual recipe is perhaps slightly closer for $\theta_{0.95}$.

Both the analytic models and the numerical simulations show that the flow becomes spherical more than a decade in time after it becomes subrelativistic (which may be quantified as the time when $\langle u\rangle_E = 1$). This can be attributed to the fact that once the flow becomes subrelativistic, its sound speed quickly drops, and so does the rate of lateral expansion. Moreover, as the flow gradually becomes more spherical, the lateral gradients become smaller, which makes the flow approach spherical symmetry more slowly.

The numerical simulations show that θ_f corresponding to lower energy percentiles (or f-values) approach their asymptotic values for a spherical flow at later times. This shows that the transfer of energy to larger θ-values is the slowest near the centre of the jet and larger near its edges, which may in turn be attributed to the lateral gradient (say of ϵ) in the jet, which are smallest near its centre and largest near its edge.

7 DISCUSSION

In this work we have introduced a new, physically motivated recipe for the lateral expansion of the jet (in Section 3). It is based on the jump conditions for oblique shocks of arbitrary 4-velocity, which imply that the velocity of fluid just behind the shock front (in the downstream region) is in the direction of the local shock normal (i.e. perpendicular to the shock front at that location; $\hat{\boldsymbol{\beta}} = \hat{\boldsymbol{n}}$, equation 9) in the upstream rest frame (which in our case is identified with the rest frame of the external medium and the central source). Our new recipe for the lateral expansion rate of the jet ($\beta_\theta \sim 1/\Gamma^2\theta_j$, equation 11) has an extra factor of $\Gamma\theta_j$ in the denominator relative to the usual recipe that has been used so far ($\beta_\theta \sim 1/\Gamma$, equation 8). This results in slower lateral expansion relative to the usual (or old) recipe at early times when $\Gamma > \theta_j$, but faster lateral expansion at later times when $\Gamma < \theta_j$, i.e. once the lateral expansion becomes significant.
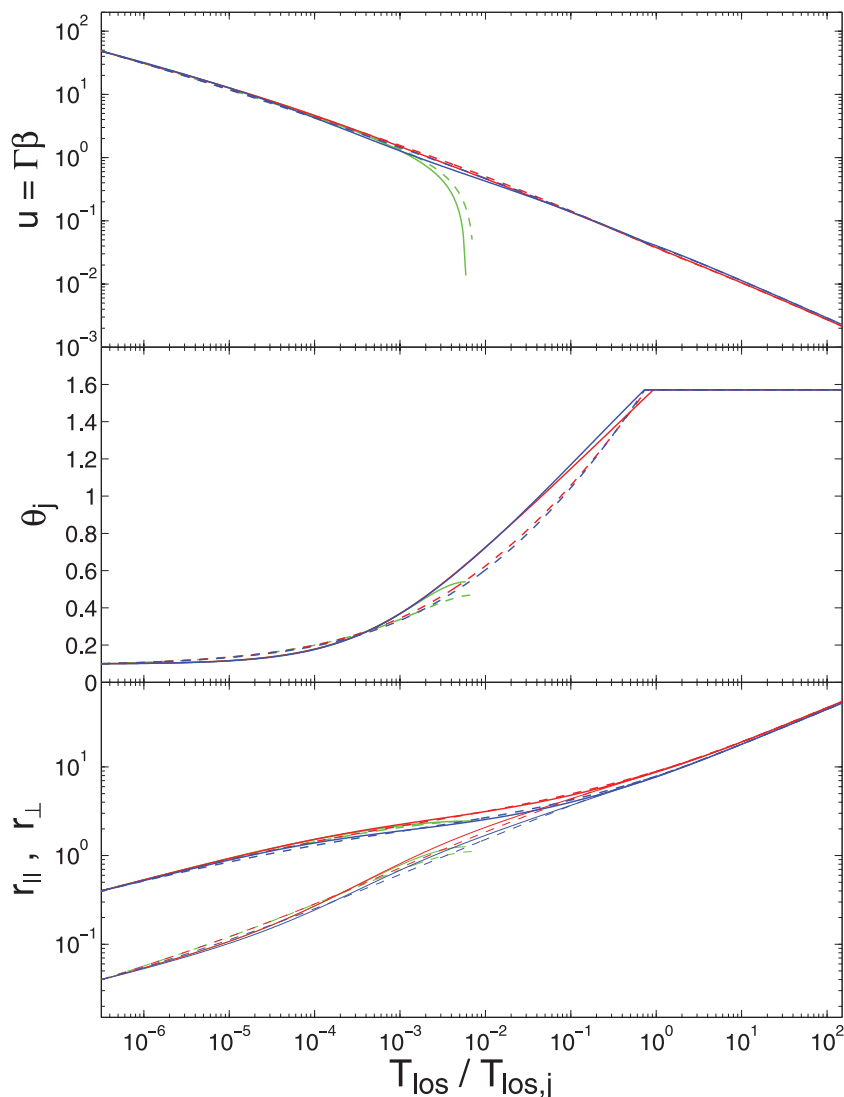
Figure 10. Similar to Fig. 9 but as a function of the observed time, $T_{\rm los}$, at which photons from the head of the jet reach an observer located along its symmetry axis, normalized by its value at the jet break time $T_{\rm los,j}$.

Next (in Section 4), we have implemented our new recipe as well as the old recipe in a simple analytic model for the jet dynamics, which is valid only for high Lorentz factors ($\Gamma \gg 1$) and narrow jet half-opening angles ($\theta_{\rm j} \ll 1$). This model shows an exponential lateral expansion for $\Gamma < \theta_0$, like previous analytic models of this type. However, we demonstrate that for typical values of the initial jet half-opening angle ($0.05 \lesssim \theta_0 \lesssim 0.2$) this model is valid only over a very limited dynamical range for $\Gamma < \theta_0$, so that the asymptotic exponential lateral expansion regime is hardly reached before the model breaks down. This leads to a reasonable agreement with numerical simulations over this limited range (as shown by Wygoda et al. 2011, and in Section 6).

This motivated us (in Section 5) to generalize our relativistic model so that it would be valid for any values of Γ and $\theta_{\rm j}$. This was done by switching to the 4-velocity u (instead of Γ) as the dynamical variable that we evolve (so that it would vary significantly in both the relativistic and the Newtonian regimes), and systematically not relying on any relativistic or small angle approximations. Moreover, we have implemented two different assumptions for the accumulation of the swept-up external rest mass, corresponding to

a different variant of the model. The trumpet model makes the usual assumption that the working surface is the part of a sphere of radius R within a cone of half-opening angle $\theta_{\rm j}(R)$. The conical model assumes that all the mass within a cone of half-opening angle $\theta_{\rm j}(R)$ was swept-up, so that once the flow becomes spherical the swept-up mass is equal to that originally within a sphere of the same radius.

Our relativistic, trumpet and conical models all agree at early times when the jet is still highly relativistic, narrow and hardly expanded sideways ($\Gamma > \theta_0^{-1} \gg 1$). At this stage the approximations of our relativistic model hold well, and there are only very small differences in the swept-up mass between the trumpet and conical models. However, at later times when $\Gamma < \theta_0^{-1}$ the relativistic model enters a phase of rapid, exponential sideways expansion and it quickly breaks down, before becoming spherical. We note, however, that for a stratified or stellar wind like external medium ($k = 2$) the jet is closer to being spherical than for a uniform or interstellar medium like external medium ($k = 0$; see bottom panel of Fig. 5) when the relativistic model breaks down.

For the trumpet and conical models, which are valid for any Γ or $\theta_{\rm j}$, the phase of rapid, exponential sideways expansion largely
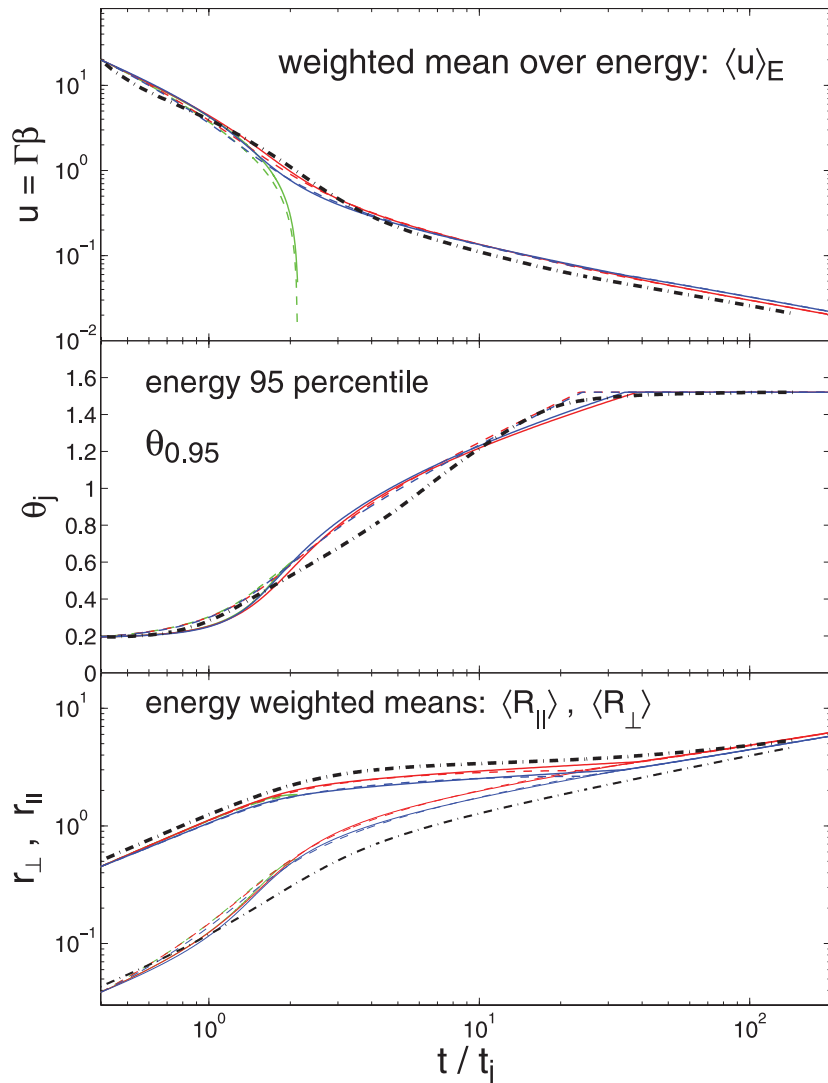
Figure 11. Comparison, for $\theta_0 = 0.2$ and $k = 0$, between our analytic models (thin lines) and the results of 2D special relativistic hydrodynamic simulations (from De Colle et al. 2011a,b) of a jet with initial conditions of a conical wedge of half-opening angle θ_0 taken out of the Blandford & McKee (1976) self-similar solution (thick dot–dashed black line), in terms of the jet 4-velocity (u), half-opening angle (θ_j) as well as normalized parallel ($r_\parallel$) and perpendicular ($r_\perp$) sizes. The green, red and blue lines are for our relativistic, trumpet and conical models, respectively. Thin solid lines are for our new recipe for lateral expansion ($a = 1$), while thin dashed lines are for the old recipe ($a = 0$).

disappears for typical values of $\theta_0 \gtrsim 0.05$. This occurs because the jet is no longer ultrarelativistic soon after Γ drops below θ_0^{-1}, and once it becomes mildly or subrelativistic its sound speed and therefore its rate of lateral expansion decrease compared to the ultrarelativistic regime. The conical model evolves somewhat faster than the trumpet model, since it accumulates external rest mass also from the sides of the jet, and thus it slows down faster. The smaller Γ results in turn in even faster lateral expansion rate and a larger θ_j (at a given radius R or lab frame time t).

We compared (in Section 6) our analytic models to the results of 2D special relativistic hydrodynamic simulations (from De Colle et al. 2011a,b), finding that they provide a reasonable description of the numerical results at all times. Therefore, they can be used for analytic calculations of the afterglow emission, and would provide more realistic results compared to previous analytic models. The main factor that significantly improves the agreement with simulations compared to previous analytic models is the fact that we have generalized the model to be valid also at modest Lorentz factors Γ

and large jet half-opening angles θ_j. Both our analytic generalized (trumpet and conical) models and the numerical simulations show that the jet first becomes subrelativistic and only then gradually approaches spherical symmetry over a long time.

For typical initial half-opening angles ($\theta_0 \gtrsim 0.05$) the phase of rapid exponential lateral spreading is largely eliminated, and it is replaced by a quasi-logarithmic increase in θ_j with radius R or lab frame time t. van Eerten & MacFadyen (2011) have stressed that while noticeable sideways expansion starts for $\Gamma < \theta_0^{-1}$, this initially involves only a small fraction of the total jet energy in its outer parts, and the central parts of the jet that carry most of its energy take longer to start spreading their energy to wider angles. While it is true that the jet does not remain uniform, the differences in the early growth of the angles θ_f containing different fractions f of the jet energy, normalized by their initial value, are not very large – less than a factor of 2 in lab frame time or radius between $f = 0.95$ and 0.5, and tend to become smaller for narrower θ_0. This can be seen from fig. 4 of van Eerten et al. (2011b), which also shows
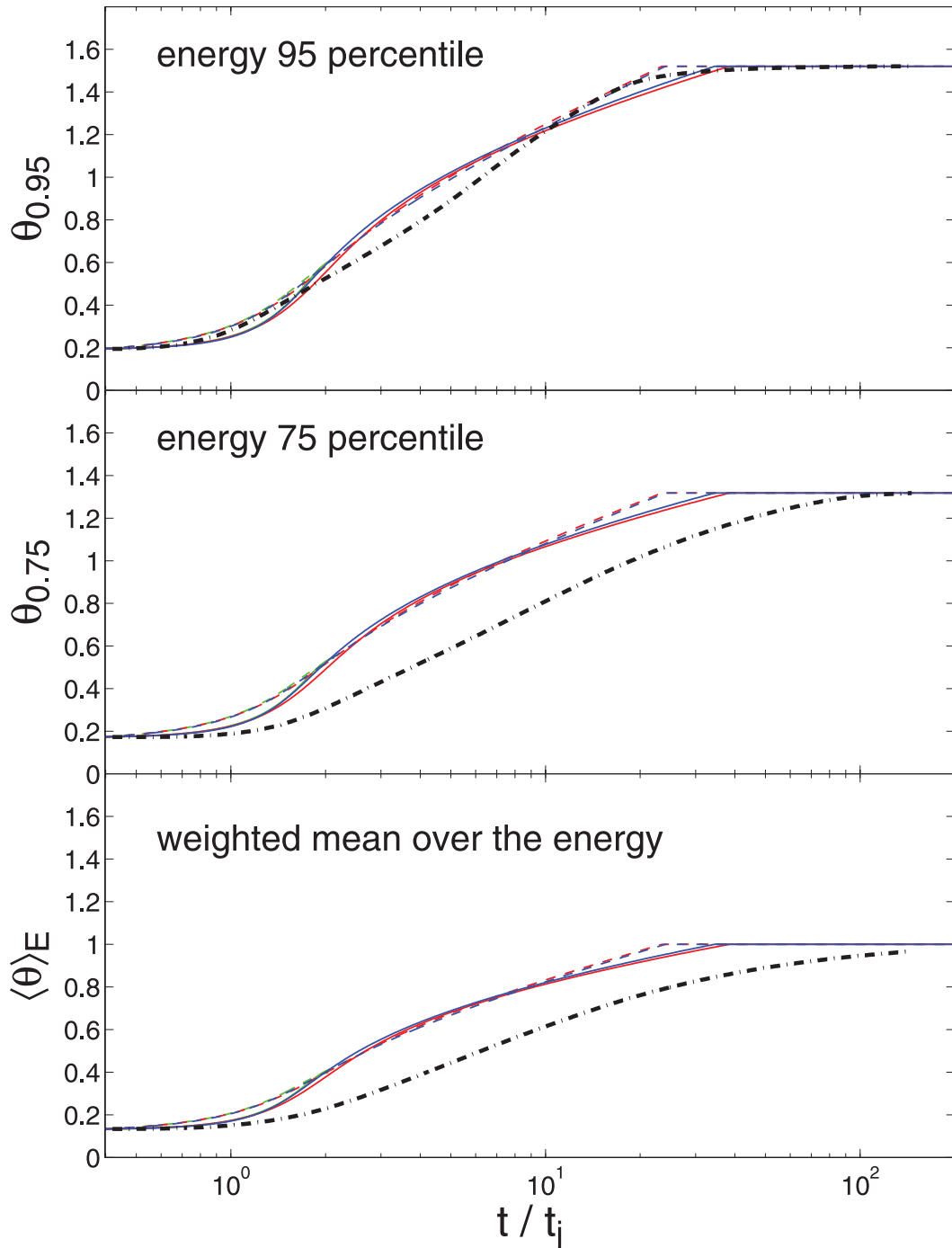
Figure 12. Similar to Fig. 11 but for three different ways of quantifying the jet half-opening angle, θ_j. The top and middle panels show two different energy percentiles, $\theta_{0.95}$ and $\theta_{0.75}$, respectively, i.e. the values of θ up to which 95 and 75 per cent of the energy is contained. The bottom panel shows the weighted mean over the energy, $\langle\theta\rangle_E$.

that as θ_0 is gradually decreased down to 0.05, its initial growth becomes steeper and it looks as if an early phase of exponential growth starts to develop, contrary to what is claimed in van Eerten & MacFadyen (2011). Therefore, we conclude that (i) although the uniform jet approximation used in our analytic models is obviously rather crude, it nonetheless provides a reasonable description of the energetically dominant part of the jet; and (ii) the prediction of our analytic models that an early exponential sideways expansion phase should exist for sufficiently small θ_0 is not only consistent with the existing simulations, but these simulations even show a hint for the

development of such a phase. This should obviously be tested more thoroughly by simulations that reach even lower values of θ_0.

A phase of exponential lateral spreading was first found by Rhoads (1999) and Piran (2000) using a simple analytic model. Later, Gruzinov (2007) found a self-similar solution with a similar scaling. Our main conclusion (which is in agreement with Wygoda et al. 2011) is that such a phase will occur in practice only for jets that are initially extremely narrow (with $\theta_0 \ll 0.05$ or so), while for more modest values of $\theta_0 \gtrsim 0.05$ that are more typically inferred in GRB jets, such a phase effectively does not exist. This basically

reconciles the long-lasting apparent discrepancy between analytic models and numerical simulations.

REFERENCES

Abdo A. A. et al., 2009, Sci, 323, 1688
Blandford R. D., McKee C. F., 1976, Phys. Fluids, 19, 1130
Cannizzo J. K., Gehrels N., Vishniac E. T., 2004, ApJ, 601, 380
De Colle F., Granot J., Ramirez-Ruiz E., Lopez-Camara D., 2011a, ApJ, in press
De Colle F., Ramirez-Ruiz E., Granot J., Lopez-Camara D., 2011b, ApJ, preprint (arXiv:1111.6667)
Frail D. A., Kulkarni S. R., Nicastro L., Feroci M., Taylor G. B., 1997, Nat, 389, 261
Fruchter A. S. et al., 1999, ApJ, 519, L13
Granot J., 2007, Rev. Mex. Astron. Astrofis., 27, 140
Granot J., Ramirez-Ruiz E., 2011, in Kouveliotou C., Woosley S. E., Wijers R. A. M. J., eds, Gamma Ray Bursts. Cambridge Univ. Press, Cambridge, preprint (arXiv:1012.5101)
Granot J., Miller M., Piran T., Suen W. M., Hughes P. A., 2001, in Costa E., Frontera F., Hjorth J., eds, GRBs in the Afterglow Era. Springer-Verlag, Berlin, p. 312
Granot J., Ramirez-Ruiz E., Loeb A., 2005, ApJ, 618, 413
Gruzinov A., 2007, preprint (arXiv:0704.3081)
Halpern J. P. et al., 2000, ApJ, 543, 697
Harrison F. A. et al., 1999, ApJ, 523, L121
Kompaneets A. S., 1960, Soviet Phys. Doklady, 5, 46
Kulkarni S. R. et al., 1999, Nat, 398, 389
Kumar P., Granot J., 2003, ApJ, 591, 1075
Kumar P., Panaitescu A., 2000, ApJ, 541, L9
Laumbach D. D., Probstein P. F., 1969, J. Fluid Mech., 35, 53
Lyutikov M., 2011, preprint (arXiv:1106.0025)
Meliani Z., Keppens R., 2010, A&A, 520, L3
Moderski R., Sikora M., Bulik T., 2000, ApJ, 529, 151
Oren Y., Nakar E., Piran T., 2004, MNRAS, 353, L35
Panaitescu A., Mészáros P., 1999, ApJ, 526, 707
Perna R., Vietri M., 2002, ApJ, 569, L47
Pihlström Y. M., Taylor G. B., Granot J., Doeleman S., 2007, ApJ, 664, 411
Piran T., 2000, Phys. Rep., 333, 529
Piran T., 2005, Rev. Modern Phys., 76, 1143
Price P. A. et al., 2001, ApJ, 549, L7
Rhoads J. E., 1997, ApJ, 487, L1
Rhoads J. E., 1999, ApJ, 525, 737
Sari R., Piran T., Halpern J., 1999, ApJ, 519, L17
Shapiro P. R., 1979, ApJ, 233, 831
Tan J. C., Matzner C. D., McKee C. F., 2001, ApJ, 551, 946
Taylor G. B., Frail D. A., Beasley A. J., Kulkarni S. R., 1997, Nat, 389, 263
Taylor G. B., Frail D. A., Berger E., Kulkarni S. R., 2004, ApJ, 609, L1
van Eerten H. J., MacFadyen A. I., 2011, preprint (arXiv:1105.2485)
van Eerten H. J., Zhang W., MacFadyen A., 2010, ApJ, 722, 235
van Eerten H. J., Meliani Z., Wijers R. A. M. J., Keppens R., 2011a, MNRAS, 410, 2016
van Eerten H. J., van der Horst A., MacFadyen A. I., 2011b, preprint (arXiv:1110.5089)
Wygoda N., Waxman E., Frail D. A., 2011, ApJ, 738, L23
Zhang W., MacFadyen A. I., 2009, ApJ, 698, 1261

APPENDIX A: COMPARISON TO PREVIOUS WORKS

We compare here our formulation for the jet lateral expansion rate, equation (11), with earlier work. This formula was first derived within the context of GRBs by Kumar & Granot (2003), who provided two different derivations. The first follows our line of argument and is based on the orthogonality of the shock front and the velocity of the fluid just behind it in the rest frame of the fluid ahead of the shock (equation 9). The second derivation involves an analysis of the dynamical equations integrated over the radial profile.

A result similar to equations (10) and (11) was also recently derived by Lyutikov (2011), based on an earlier work by Shapiro (1979). Lyutikov (2011) has argued that it implies a negligible lateral expansion as long as $\Gamma \gg 1$ unless $\Delta\theta < 1/\Gamma^2$, suggesting that with this model one obtains a slow sideways expansion, as seen in the numerical simulations. However, we note that the condition $\Delta\theta < 1/\Gamma^2$ corresponds to $\beta_\theta \sim 1$. This requirement is too extreme since $\beta_\theta \sim 1$ would result in a quasi-spherical flow within a single dynamical time (since in that case $\beta_\theta \gtrsim \beta_r$). As is well known (see also Section 4), the traditional recipe for lateral expansion (equation 8), namely $\beta_\theta \sim 1/\Gamma$, already gives an asymptotic exponential growth of θ_j with R (i.e. very rapid lateral expansion).

The earlier work by Shapiro (1979) discusses two possible approximations for the dynamics of a non-spherical relativistic blast wave, both based on a thin shell approximation for the layer of shocked external medium that carries most of the energy, but with different additional assumptions: (i) the quasi-radial approximation (used in the Newtonian regime by Laumbach & Probstein 1969) in which each part of the shock is assumed to move in a radial trajectory as if it were part of a spherical flow with the same local conditions (and in particular the same energy per solid angle, excluding rest energy, $\epsilon = \mathrm{d}E/\mathrm{d}\Omega$); and (ii) the Kompaneets (1960) approximation that the pressure behind the shock is uniform, i.e. the same at all locations behind the shock and is proportional to the average energy density in the region bounded by the shock front. The first approximation assumes that the energy per solid angle in the flow (excluding rest energy) does not change and remains equal to its initial value, $\epsilon(t, \theta) = \epsilon(t_0, \theta)$. In this sense, it basically assumes no lateral expansion (as the jet retains its initial angular structure in $\epsilon(\theta)$ indefinitely), so that this is a model assumption in this case rather than a result.

The second approximation, which was originally used by Kompaneets (1960) in the Newtonian regime, does not appear to be very appropriate for the relativistic regime where the angular size of causally connected regions is $\sim 1/\Gamma \ll 1$, so that the local dynamics of a small portion of the flow should not be affected by the average energy per unit volume in the whole flow, which may be dominated by regions that are not in causal contact with it. A simple example of how the Kompaneets (1960) approximation violates causality in the relativistic regime is that for a uniform external medium, it implies that the velocity of the shock front is uniform (i.e. depends only on the lab frame time, but not on the location along the shock front; Shapiro 1979), which necessarily implies that the flow must approach spherical symmetry within a few dynamical times.[6] This

---

[6] The direction of the velocity of the fluid just behind the shock, which is along the shock normal, might be initially non-radial, but since the shock velocity is the same everywhere and highly relativistic, it quickly approaches spherical symmetry, similar to the wave left by a stone thrown into water, where the velocity of the surface water wave is uniform and the wave front quickly forgets the shape of the stone and becomes circular as its radius becomes larger than that of the stone. In our case, within a few dynamical times ϵ becomes essentially independent of θ, since its local value is dominated by the recently shocked material, where the shock Lorentz factor is uniform.

obviously violates causality, since as we discussed in the Section 1, a roughly uniform jet with reasonable sharp edges cannot expand sideways significantly as long as $\Gamma\theta_0 \gg 1$, from causal considerations (since its bulk is not in causal contact with its edges, and it does not 'know' that it is not part of a spherical flow and should thus start expanding sideways).

Shapiro (1979) reaches the conclusion that the two approximations give the same result in the extreme relativistic limit only because he explicitly assumed that in the quasi-radial approximation, the energy per solid angle, $\epsilon = \mathrm{d}E/\mathrm{d}\Omega$, is not only independent of time, but also of the location along the shock front (this can be seen from the fact that his energy integral is independent of θ). This assumption quickly leads to a quasi-spherical flow for a spherical external density profile, and the non-spherical solutions obtained by Shapiro (1979) arise since he considered an exponential atmosphere, which is a highly non-spherical external density profile. The problem of interest for us, namely the dynamics of GRB jets during the afterglow phase, involves a non-uniform initial distribution of the energy per solid angle, $\epsilon(t_0, \theta)$, and in such a case the two approximations are not equivalent in the extreme relativistic limit. Therefore, we conclude that neither of these two approximations appears to be appropriate for studying the dynamics or degree of lateral spreading of GRB jets during the afterglow phase.

This paper has been typeset from a TeX/LaTeX file prepared by the author.